ABSTRACT

Title of Document:	INTERACTION OF INTENSE SHORT LASER PULSES WITH GASES OF NANOSCALE ATOMIC AND MOLECULAR CLUSTERS.
	Ayush Gupta, Ph.D., 2006
Directed By:	Professor Thomas M. Antonsen, Jr., Department of Electrical and Computer Engineering

We study the interaction of intense laser pulses with gases of van der Waals bound atomic aggregates called clusters in the range of laser-cluster parameters such that kinetic as well as hydrodynamic effects are active. The clustered gas absorbs the laser pulse energy efficiently producing x-rays, extreme ultraviolet radiation, energetic particles and fusion neutrons.

First, we investigate the effect of pulse duration on the heating of a single cluster in a strong laser field using a 2-D electrostatic particle-in-cell (PIC) code. Heating is dominated by a collision-less resonant absorption process that involves energetic electrons transiting through the cluster. A size-dependent intensity threshold defines the onset of this resonance [Taguchi et al., Phys. Rev. Lett., v90(20), (2004)]. It is seen that increasing the laser pulse width lowers this intensity threshold and the energetic electrons take multiple laser periods to transit the cluster instead of one laser period as previously recorded [Taguchi et al., Phys. Rev. Lett.,

v90(20), (2004)]. Results of our numerical simulations showing the effect of pulse duration on the heating rate and the evolution of the electron phase space are presented in this dissertation. Our simulations show that strong electron heating is accompanied by the generation of a quasi-monoenergetic high-energy peak in the ion kinetic energy distribution function. The energy at which the peak occurs is pulse duration dependent. Calculations of fusion neutron yield from exploding deuterium clusters using the PIC model with periodic boundary conditions are also presented.

We also investigate the propagation of the laser pulse through a gas of clusters that is described by an effective dielectric constant determined by the single cluster polarizability. For computational advantage, we adopt a uniform density description of the exploding clusters, modified to yield experimentally consistent single cluster polarizability, and couple it to a Gaussian description of the laser pulse. This model is then used to study self-focusing, absorption, and spectral broadening of the laser pulse. The model is further extended to allow for a fraction of the gas to be present as unclustered monomers and to include the effect of unbound electrons produced in the laser-cluster interaction.

INTERACTION OF INTENSE SHORT LASER PULSES WITH GASES OF NANOSCALE ATOMIC AND MOLECULAR CLUSTERS

By

Ayush Gupta

Dissertation submitted to the Faculty of the Graduate School of the
University of Maryland, College Park, in partial fulfillment
of the requirements for the degree of
Doctor of Philosophy
2006

Advisory Committee:
Professor Thomas M. Antonsen, Jr., Chair
Professor H.M. Milchberg
Associate Professor Thomas Murphy
Dr. Parvez Guzdar
Professor Rajarshi Roy

Dedication

To my parents

Acknowledgements

It was the mentorship, guidance, patience and support of a lot of people that made this work possible.

Prof. Antonsen has been an excellent advisor throughout the period of this work. He guided me with a gentle hand providing technical assistance where needed and inspiration always. His personal discipline, academic brilliance and wonderful mentorship have left an indelible impression on my mind. Without his support this work could not have been completed. I would like to thank Dr. Toshihiro Taguchi, visitor to our group from Japan, for valuable discussions on my research problem, for teaching me the use of the PIC code used in this dissertation and for help with actually running the code on various computer systems. I am really grateful to him for his guidance, often from Japan over email. I would like to acknowledge Dr. Parvez Guzdar who acted as a mentor for me. He gave valuable guidance to me about the project as well as advice regarding careers. Conversations with him helped me form a better outlook towards science and research. For that, I am indebted to him. I am very thankful to Dr. Milchberg for the many conversations I had with him during the course of my graduate school. I learnt a lot while collaborating with him. I am also indebted to him for helping me navigate the process of coming out while in graduate school, a very crucial personal issue that had threatened the very course of my Ph.D.

I am thankful to all my committee members for taking the time to meet with me to discuss this work and for reading the thesis.

I would like to thank Prof. Bill Dorland for valuable assistance with

programming issues and for granting me access to the Beo-wolf cluster.

I would like to thank my fellow graduate students, Paul Cassak, Muralidhar Yeddulla, John Palastro for valuable discussions on physics as well as socio-political topics. I thank previous graduate students in our group, Dr. Jianzhou Wu, and Dr. Jim Cooley for provided computational assistance. I thank my friends in graduate school, in particular Brinda Ganesh and Ayan Roy Chowdhury for providing support through the graduate school existence. I would also like to thank Prof. Amit Roy Chowdhury (ECE alumnus) for his valuable guidance on general research and technical writing issues in the early phase of this work.

This work would not have been possible without the support and assistance of the diligent staff at IREAP and the ECE Department. Ed Condon was very prompt in his help with everything about managing the computer facilities in the office. Mohini and Janet were very helpful with travel arrangements and office supplies. Nancy (IREAP) and Maria Hoo (ECE) were very helpful with the paperwork for taxes and student requirements. I thank them all.

Finally, I would like to thank my partner, Theron and my parents for their love, support, and patience throughout this process.

Table of Contents

List of Tables

List of Figures

quasimonoenergetic peak of ions dominates the ion distribution function. The energy at which this peak occurs is pulse duration dependent. For both electron and ions, the distribution functions show an increase in energy as the pulse length is increased from 100 fs to 250 fs, but in either case the energy falls down as the pulse length is further increased to 1 ps.

Fig 2.8 Ion kinetic energy distribution functions under periodic boundary conditions for deuterium ions of initial diameter 38nm irradiated with laser pulses of 100fs duration and peak intensities of (a) 1×10^{15} W/cm^2, (b) 3×10^{15} W/cm^2, (c) 1×10^{16} W/cm^2, (d) 5×10^{16} W/cm^2, and (e) 1×10^{17} W/cm^2.

Fig 2.9 Fusion reaction rate per unit volume (left vertical axis) and total neutron yield (right vertical axis) as a function of peak laser intensity for deuterium clusters with D_0 = 38nm.

Fig 3.1 A comparison of the real and imaginary polarizability for our model (a,b) and the hydrocode of Milchberg (c,d). In each case, a cluster of initial radius 30nm is irradiated with a 800nm, 100 fs FWHM laser pulse for three different peak intensities 5×10^{14} W/cm^2 (dashed), 8×10^{14}W/cm^2 (dotted), and 1×10^{15} W/cm^2 (solid - dark). The pulse profile is shown in (a) as a thin solid line.

Fig 3.2 Contour plot of (a) real and (b) imaginary part of polarizability in the r-ξ plane. The ellipse in the center of each plot marks FWHM points.

Fig 3.3 The quantities $H_r(\xi=0$ fs) (solid) and $H_i(\xi=0$ fs) (dashed with cross markers) are plotted at z = 0.006 cm. Here, the cluster density set to $n_c = 3\times10^{11}$ cm^{-3} and the spot size of the pulse was varied from 10μm to 200μm. All other parameters were initialized to the conditions in Table 3.1. The intersection of H_r with the $1/k_0R_0^2$ curve (dashed) gives the equilibrium values of R for the chosen cluster density

Fig 3.4 Cluster density required for equilibrium of a pulse as a function of the pulse spot size for three different initial energies 1.93 mJ (dash-sot), 9.65 mJ (dashed), and 19.3 mJ (solid). All other parameters were initialized to the conditions in Table 3.1. Note that for a pulse with given initial energy the same cluster density can occur for two values of R

Fig 3.5 Stability expression $(2H_r + R\partial H_r/\partial R)_{R=R0}$ vs. spot size R for a laser beam for three different initial pulse energies 1.93 mJ (dash-dot), 9.65 mJ (dashed), and 19.3 mJ (solid) All other parameters initialized to the conditions in Table 3.1. The range of R over which the plotted quantity is positive is stable. For example, in the 1.93mJ case, the region of stability corresponds to 14μm<R<82μm and R<8μm

Fig 3.6 Power within the pulse (initial parameters of Table 3.1) at z = 0cm, 0.3 cm, 0.6cm, 0.9 cm and 1.2 cm. The front of the pulse, traveling through unionized clusters, does not get absorbed and hence propagates unattenuated while the trail end

(where the imaginary part of polarizability is high) is strongly attenuated.

Fig 3.7 Self-guiding of the laser pulse in cluster medium. The figure shows the spot size at the center of the pulse ($\xi = 0$ fs) (dashed with square marker) for propagation through 2.0 cm of clustered gas for the initial conditions of Table 3.1. The result for propagation through vacuum (solid with circle markers) is plotted for comparison. The RMS (root mean squared) spot size is also shown (dashed with diamond markers). The center of the pulse remains focused for roughly 1.5cm. The energy within the pulse (solid with cross markers) is plotted in mJ (right axis). We note that about 83% of the pulse energy is absorbed by the clusters in 1.5 cm of propagation, after which the rate of absorption levels off.

Fig 3.8 RMS spot sizes as a function of propagation distance for pulses with six different initial peak intensities: 5×10^{14} W/cm^2, 8×10^{14}W/cm^2, 1×10^{15} W/cm^2, 2×10^{15} W/cm^2, 5×10^{15} W/cm^2, and 1×10^{16} W/cm^2. Here cluster density was set to $n_c = 3\times10^{11}$ cm^{-3}, other initial conditions being those in Table 3.1. We note that the guiding effect is strongest around peak intensity of 2×10^{15} W/cm^2. The evolution of spot size for a pulse propagating in vacuum is plotted for comparison.

Fig 3.9 Variation of energy within the pulse with propagation for pulses of different initial peak intensities: 5×10^{14} W/cm^2, 8×10^{14}W/cm^2, 1×10^{15} W/cm^2, 2×10^{15} W/cm^2, 5×10^{15} W/cm^2, and 1×10^{16} W/cm^2. Here cluster density was set to $n_c = 3\times10^{11}$ cm^{-3}, other initial conditions being those in Table 3.1. Pulses with higher initial energy have a higher rate of energy absorption initially. As the pulse energy gets depleted the rate of absorption falls.

Fig 3.10 (a) Phase, (b) chirp developed, (c) spot size of the pulse, (d) radially averaged frequency shift, and (e) power weighted radial averaged frequency shift, at z = 0.3 cm, 0.72 cm, and 0.9 cm (for initial conditions of Table 3.1). The rise in phase at ξ =-80 fs is due to ionization and appears in (b) and (d) as a red shift. The z = 0.72 cm curve shows a kink in phase at around ξ= 86 fs. This is due to the sharp focusing of the pulse as seen in (c) and provides further red shift as seen in (b) and (d). The frequency shift weighted with power gives the effect of the propagation on the pulse spectrum.

Fig 3.11 Variation with propagation distance of spot size (a), curvature (b) and phase (c) of the pulse at three different locations within the pulse (ξ= 0 fs, 86 fs, 101 fs). The moving focus seen in (a) causes a sharp fall in phase (c).Fig 3.12 Power spectrum of the pulse (in logarithmic scale) for $z = 0$ cm, 0.3 cm and 0.9 cm. We see the spectrum broadening with propagation and significant red shifting of the initial spectrum..

Fig 3.12 Power spectrum of the pulse (in logarithmic scale) for $z = 0$ cm, 0.3 cm and 0.9 cm. We see the spectrum broadening with propagation and significant red shifting of the initial spectrum.

Fig 4.1 Experimental layout for the measurement of forward and side

scattered spectra of intense laser pulses interacting with a gas of clusters.

Fig 4.2 Mean wavelength of (a) scattered and (b) transmitted laser pulses as a function of chirped laser pulse durations. The mean wavelength of incident lasers is 798 nm. The insets show sample 1D space-resolved (a) scattering and (b) transmission spectra, respectively.

Fig 4.3 Simulated mean wavelength of transmitted laser pulses as a function of chirped laser pulse durations for different assumed fraction of gas atoms present as clusters.

Fig 4.4 The dotted line shows the evolution of free electron density with time within the pulse for peak laser intensity of 6×10^{15} W/cm^2 (the laser pulse envelope is shown in thin solid line). The energy absorbed per electron based on the PIC calculations for the same laser peak intensity is also shown (solid line).

Fig 4.5 Comparison of real (a,b) and imaginary (c,d) parts of cluster polarizability from the PIC code (solid lines) and modified uniform density model of cluster expansion with inclusion of hot electrons (dotted lines) for a range of intensities. For the PIC code the polarizability is normalized to $\gamma_0 = D_0^2/8$, where D_0 is the diameter of the cluster while for the uniform density model it is normalized to $\gamma_0 = D_0^3/8$.

Fig 4.6 RMS spot size of pulse for case when free electrons are included (circles) and when free electrons are not considered (filled circles). The evolution of the RMS spot size for propagation in vacuum is plotted (solid-no marker) for comparison. The free electrons contribute additional defocusing effect.

Fig 4.7 RMS spot size of the pulse versus distance of propagation for a range of peak laser intensities. The RMS spot size for propagation in vacuum and through unclustered gas at a peak intensity of 1×10^{17} W/cm^2 is also plotted for comparison. We note that the RMS spot size is higher for higher intensity at any given distance. This is due the generation of more free electrons at higher intensities. However, even for the peak intensity of 1×10^{17} W/cm^2 the RMS spot size is less than that for propagation in vacuum.

1 Introduction

1.1 Overview

Clusters are nanoscale solid density atomic aggregates bound by van der Waals forces ranging in size from $10^2 – 10^6$ atoms. Clusters can be made from different atomic, molecular and hetero-nuclear species. In this thesis, we look only at clusters formed from gases such as argon, xenon, and deuterium. Gas-atom clusters are formed when high-pressure flow of a cooled gas into vacuum results in adiabatic cooling and expansion of the gas and particle aggregation [1]. A clustered gas jet typically consists of solid density clusters along with low-density background of un-clustered gas atoms. Clusters vary in size from a few angstroms to a 1000Å in diameter and the density of clusters in the gas ranges typically from 10^{11} to 10^{14} clusters/cm^3. The characteristics of the clustered gas such as the size distribution and number density of clusters and the ratio of clusters to un-clustered atoms or molecules is determined by the backing temperature, pressure, nozzle geometry and other experimental factors.

When irradiated by an intense laser pulse, clusters absorb energy and explode, leaving behind tenuous plasma. The volume average density of the clustered gas is low but the clusters themselves are at solid density. This enables strong interaction of individual clusters with an irradiating laser pulse while still allowing propagation of the pulse through the clustered gas. The efficient coupling of laser energy into

clustered gases [2] makes them a unique media for studying non-linear laser-matter interaction [3] and can lead to many exciting applications.

The laser-heated clusters efficiently generate x-ray [4] and extreme ultraviolet (EUV) radiation [5-9] with yields comparable to that from interaction of intense laser pulses with planar solid targets. Clusters have the advantage that they do not generate debris, which is an issue with solid targets and the system takes much less space than the conventional synchrotron radiation source. Clusters irradiated with strong laser pulses can thus be used as an easily-renewable, debris-free tabletop radiation source for such applications as X-ray lasers, X-ray and EUV lithography [5] and X-ray tomography [10]. Explosion of clusters in strong laser fields leads to ejection of high energy electrons and energetic highly charged ions [11-13]. This opens up the possibility of using energetic particles from laser-irradiated clusters to seed particle accelerators and for proton beam radiation therapy in cancer treatment [14]. Collisions between energetic ions from exploding clusters can produce neutrons via thermonuclear fusion [12, 15]. Laser irradiated clusters can thus be a future tabletop source of thermonuclear neutrons for imaging purposes. The dynamics of exploding clusters gives rise to interesting nonlinear optical effects such as harmonic generation [16] and self-focusing [17]. Clustered gases are also proposed as targets for creating plasma waveguides [18, 19]. Self-guiding of a laser pulse in plasma and plasma channel formation are of particular interest for laser-based particle acceleration schemes.

Understanding the dynamics of laser-cluster interaction and cluster explosion is a challenging experimental and theoretical problem with the intellectual reward of

providing insight into the behavior of molecular assemblies in strong electromagnetic fields and is also necessary for optimizing the system for the above-mentioned applications. Strong absorption of laser pulse energy by clusters is the central enabling feature for these applications. As such the first part of this thesis focuses on laser pulse energy absorption by an individual cluster via simulations of a kinetic description of the cluster plasma. We examine the role of laser intensity and pulse duration in determining the manner of laser to cluster energy coupling for argon and deuterium clusters. Subsequently, we use a hydrodynamic description of expanding heated cluster to model the interaction of laser pulses with extended clustered gas medium. This work has been motivated by the current advances in experiments on laser-cluster interactions and has built upon the past theoretical models of cluster heating and expansion. A survey of some of the experimental and theoretical studies on this topic is presented in Sections 1.2 and 1.2, followed by a brief description, in Sections 1.4 and 1.5, of the specific questions explored in this dissertation.

1.2 Experimental Studies

Laser-cluster interaction first shot into prominence with the observation of strong emission of X-rays from laser-irradiated xenon clusters [20-24]. Subsequently, other groups have measured and characterized the emission of strong X-rays [25-36] and extreme ultraviolet (EUV) radiation [5-9] from gas clusters subjected to a high intensity laser pulse. Clustered gases, having properties in between that of solid and gas phase, were shown to be very efficient absorbers of laser pulse energy [2]. Further studies on laser pulses propagating through clustered gases produced interesting non-linear optical effects such as self-focusing [17], modulation of the pulse spectrum[37]

and higher harmonic generation [38, 39]. Time of flight measurements of the electrons and ions generated from exploded clusters revealed highly energetic particles being generated. Electrons with energies up to 3 keV have been observed [11] while maximum ion energies measured are of the order of 1 MeV [40]. Nuclear fusion via collisions of ions from exploded deuterium clusters has been demonstrated and the neutron yield measured [12, 15, 41]. Desire to optimize the system for potential applications such as creating a radiation, energetic particles or neutron source has led to experiments on the role of parameters pertaining to the irradiating laser pulse and the irradiated clustered gas. These studies show that the laser pulse duration, peak intensity, and wavelength as well as the cluster size, number density, material and background gas density affect cluster evolution and laser pulse propagation. While the initial laser parameters can be directly controlled, the cluster parameters such as the size distribution and number density need to be experimentally determined and is a challenging task [42]. Determination of the cluster properties is of significance to theorists since models of cluster heating indicate that the manner in which clustered gases couple to the laser energy depends strongly on the cluster size and their number density [43]. The most popular method of calculating the average cluster size is by using the Hagena parameter [1] that relates the average number of atoms in a cluster in a gas jet to the backing pressure and temperature, but it is shown to become increasingly inaccurate for larger sized clusters (number of atoms greater than 10^5). As such, Kim *el al.* [42] developed an all-optical technique to measure independently the average cluster size and the density of clusters using Rayleigh scattering imaging and interferometry but the exact form of the cluster size

distribution still eludes us. More recently, efforts towards optimizing ion-energy and the yield of fusion neutrons has prompted experiments on laser irradiation of heteronuclear clusters [44].

1.3 Heating and Expansion of Clusters: Theoretical Models

The unique nature of clustered gases as a combination of solid clusters in low density gas along with their violent interaction with high intensity laser pulses has prompted many theoretical models to explain experimental observations and model the dynamics of an exploding cluster. One of the earliest models of laser-cluster interaction was given by McPherson *et al.* [22] with the aim to explain the X-ray emission from laser-irradiated clusters. In this model, the electrons are coherently driven by the external laser field. This greatly increases the probability of ionization of inner-shell electrons resulting in 'hollow atoms' with vacant inner shells and populated outer shells. These would then decay promptly and in the process would emit X-rays. This was followed by the 'ionization ignition model' proposed by Rose-Petruck *et al.* [45] in which the external laser field and the strong electric field of the ionized cluster atoms both have a significant role in determining the ultra-fast electron dynamics and inner-shell ionization. Both models however, pertain to small clusters and focus on the ionization of the cluster with generation of very high charge state ions. For larger clusters or for high intensities a plasma model of cluster is more suitable.

Recent models of clusters as evolving balls of plasma indicate that the manner of heating and explosion of a laser-irradiated cluster has several characteristic regimes based on the laser intensity and size of cluster. Two relatively distinct

regimes are hydrodynamic expansion and Coulomb explosion. For high intensities ($> 10^{17}$ W/cm^2) or very small clusters (diameter < 25 angstroms) most electrons are removed from the cluster early in the pulse. Subsequently, the cluster explodes due to the Coulomb repulsion forces between the positively charged ions remaining in the cluster core. Typically, particle models have been used to study this regime [46-49]. In these models the electrostatic interaction between particles is treated point wise (particle to particle, also known as molecular dynamics simulations) or in the particle in cell (PIC) approximation [50]. The molecular dynamics method is suited for small clusters and becomes computationally inefficient for large clusters. The PIC method is more practical for large clusters. It is, however, relatively more difficult to describe collisions in the PIC framework.

At lower intensities and for large clusters a hydrodynamic approach is valid. Here, the expansion is driven by the pressure of electrons. In this approach, the cluster is modeled using fluid equations. The first study of hydrodynamic expansion of a cluster [51] treated the ionized cluster as a spherical ball of uniform 'nanoplasma' with no density or temperature gradients. The electrons are generated by field and collisional ionization and heated primarily by the electron-ion collisions within the cluster. For the brief time interval when the electron plasma frequency in the expanding cluster satisfies $\omega_{p0} = \sqrt{3}\ \omega_0$, where ω_0 is the laser frequency, an electrostatic resonance causes the field inside the cluster to rise sharply leading to rapid heating. This model has been very useful in explaining many aspects of cluster expansion like high ionization levels, generation of energetic ions, and resonant absorption. A more sophisticated approach allows for non-uniformity of temperature

and density during expansion [52]. This model predicts that the dominant energy absorption occurs in regions where the electron density is near the critical density. The main consequence of this is that strong absorption occurs over a much longer duration than that predicted by the uniform density model. In both these models, the response of the cluster to the laser electric field is treated in the cold plasma approximation and is used for calculation of the total electric field as well as the energy absorbed by the cluster. However, when energetic particles are produced the local cold plasma approximation no longer applies. Energetic particles travel a distance comparable to the cluster size in a laser period contributing to a non-local and non-linear dielectric response. This necessitates a kinetic treatment of the absorption process.

In recent years, some PIC models [53-56] have focused on the intermediate range of intensity and cluster sizes where a population of energetic electrons is produced and the heating and expansion of the cluster are distinctly non-hydrodynamic. However, the cluster still remains quasi-neutral as it expands. This is also the regime of interest for the present work. In this regime energy absorption by electrons is both a kinetic and a collective effect. The energetic electrons make large excursions, comparable to the size of the cluster, and being at a high temperature are largely unaffected by collisions [collision frequency is inversely proportional to temperature]. At the same time, the laser field is strongly shielded from the cluster core by the dielectric response of the electrons.

The major result of Taguchi and Antonsen [53, 54] is that there is a well defined intensity threshold above which electrons rapidly gain energy by a process

related to that proposed by Brunel for sharp density gradients [57]. Electrons are first accelerated out from the cluster and then driven back into it by the combined effects of the laser field and the electrostatic field produced by the laser-driven charge separation. The energetic electrons then pass through the cluster and emerge on the other side. If they emerge in phase with the laser field, there is resonant heating, and the cluster quickly absorbs energy. The onset of this resonance corresponds to the intensity for which the excursion of a free electron in the laser field is comparable to the cluster diameter. This critical intensity was shown to be

$$I_0 = \frac{c}{8\pi}\left(\frac{m_e\omega^2}{2\pi e}\right)^2 D_0^2 \qquad (1.1),$$

where c is the speed of light in vacuum, D_0 is the initial cluster diameter, ω is the frequency of the laser pulse and m_e and e are the electron mass and charge respectively.

In addition to these, there are other fluid and kinetic models that aim to explain specific aspects of the laser-cluster interactions such as third harmonic generation [38, 58], generation of high charged states of ions [59], self-focusing of the laser pulse [60].

1.4 Focus of this Dissertation

1.4.1 Effect of laser pulse duration on heating of a single laser irradiated cluster

In this thesis, we use the PIC framework of Taguchi and Antonsen [53] to examine how laser pulse duration influences the energy absorption by clusters. Our

simulations show that increasing the pulse duration enables strong heating via a higher order electron transit time resonance where the electron transit time through the cluster equals multiple laser periods, effectively lowering the intensity threshold for strong heating. We modify the scaling law for the intensity threshold derived in reference [53] to take the higher order electron transit time resonance into account.

Fusion of ions from exploding deuterium clusters as observed in experiments has generated interest in laser irradiated clustered gases a potential source of fusion neutrons. Some past studies [41, 44, 56, 61-63] have investigated fusion neutron yield in the Coulomb explosion regime. In the present work, we use the ion energy spectrum from our PIC model to estimate the fusion yield from deuterium clusters for a range of pulse intensities and pulse durations and examine the effect of intensity threshold on fusion yield in the regime where both kinetic and hydrodynamic effects are active.

1.4.2 Laser Pulses Interacting with Extended Clustered Gas Medium

. We have developed a self-consistent model for the propagation of an intense laser pulse in a gas of exploding clusters that acts as a non-linear optical medium. Experimental and theoretical studies of laser-irradiated clusters indicate that the clusters expand and explode even as the laser pulse is passing over them. It can thus be expected that the manner in which clusters explode would affect the propagation of the laser pulse through the extended clustered gas media. Indeed, experiments on the interaction of an intense laser pulse with cluster gas have demonstrated interesting optical effects such as the self-focusing of the laser pulse [17], strong absorption of the laser pulse energy [2], and spectral broadening of the pulse [37, 64]. In order to

understand these effects, we need a model that describes the dynamics of the laser-irradiated clusters as well as the back reaction on the laser pulse propagation due to the optical response of the cluster ensemble. However, most theoretical models of laser-cluster interaction have focused on the evolution of a single cluster in a laser field or do not consider a fully self-consistent model with a time dependent optical response of the medium and a laser pulse profile that evolves as it propagates. Computational complexity of modeling even a single cluster expansion has been a limitation and a challenge for propagation studies which require simulating a large number of clusters. To overcome this, we modeled the cluster as an expanding ball of heated plasma following reference [51] but with suitably modified parameters that we achieve an experimentally consistent optical response of the cluster without sacrificing computational speed. We couple the uniform density model, thus modified, to a Gaussian description of the laser pulse and study the propagation of a laser pulse through a cluster plasma. Our simulation results explain many experimentally observed effects like focusing and strong absorption of the laser pulse.

1.5 Organization

The organization of this dissertation is as follows. The results of our PIC simulations showing how cluster explosion dynamics change with varying pulse duration are discussed in Chapter 2. Calculations of fusion neutron yield from exploded deuterium clusters are also presented. In Chapter 3, the focus is widened to consider the effect of laser pulse propagating through an ensemble of clusters. Simulation results from our fully self-consistent calculation and comparisons to experimental results are presented in this chapter. Results of the fluid simulations to

explain the experimentally observed shifts in the mean transmitted wavelength of the laser pulse spectrum are presented in Chapter 4. Chapter 5 ends the dissertation with discussions on future work and conclusions.

2 Resonant Heating of Clusters: Effect of Pulse Duration, High Energy Ions and Neutron Yield from Fusion

2.1 Introduction

The interaction of clusters with strong laser fields is characterized by a large number of tunable parameters such as the peak intensity, pulse duration, spot size, frequency and field polarization of the laser pulse, the distribution of cluster sizes, fraction of gas present as monomers, and the density and ionization potentials of the cluster atoms. Various experimental [25, 27, 30, 43, 44, 61] and theoretical studies [52-54, 56, 63, 65] have explored the role played by some of these parameters with theoretical studies often focused on the effect of laser intensity and cluster size. Experiments show that pulse duration plays an important role in the various aspects of laser-cluster interaction such as absorption and scattering of laser pulses [66], neutron yield of deuterium cluster targets [61], x-ray generation [27] and extreme ultraviolet emission [27, 67]. In this chapter we examine the effect of laser pulse duration (Full Width at Half Maximum (FWHM) of the laser pulse envelope) on the heating of individual irradiated argon and deuterium clusters via simulations of the kinetic description of the cluster plasma. Numerical results from our simulations are discussed in Section 2.3. The range of parameters we consider is such that both hydrodynamic and kinetic effects are active. In other words, the cluster core remains quasineutral during expansion, while there is a population of energetic electrons that plays a significant role in cluster heating and expansion. In addition, we look at the yield of fusion neutrons from exploded deuterium clusters for a range of peak laser

intensities in Section 2.5. The material presented in the following sections of this Chapter has been submitted for publication [68]. The basic model and framework used for our simulations is described in the next section.

2.2 PIC Model

To study the effect of laser pulse parameters on cluster heating in the transition regime, we use a 2D electrostatic particle-in-cell (PIC) model which has been presented in detail in references [53, 54]. The laser field $E=E_x(t)sin\omega t$ is polarized in the x direction with frequency ω corresponding to λ = 800nm, and time dependent amplitude $E_x(t)$ corresponding to a Gaussian pulse. The electrostatic calculation is appropriate in the near field limit ($D_0/\lambda \ll 1$), and for intensities below $\sim 5\times10^{17}$ W/cm^2. For higher intensities, where the quiver velocity approaches the speed of light, the Lorentz force becomes important, necessitating an electromagnetic simulation.

As the intensity rises past a threshold ($\sim 10^{14}$ W/cm^2 for argon atoms) during the pulse neutral cluster atoms are ionized by field ionization followed by collisional ionization. This produces a super-critically dense plasma with electron density $n_e > n_{cr}$, where n_{cr} is the density at which the electron plasma frequency equals the incident laser frequency. The plasma shields the core of the cluster from the laser field. The majority of our simulations begin here by modeling the clusters as consisting of pre-ionized atoms and electrons. The material parameters used for argon and deuterium clusters are specified in Table 2.1. The initial temperatures in either case are chosen to be 10 eV for electrons and 0 eV for ions. This electron temperature is large enough to suppress grid instabilities inherent to PIC algorithm, but not so large as to affect

results. Electron-ion scattering processes are included explicitly in our code through a Monte Carlo method, but ion-ion and electron-electron scattering processes are neglected. Over the few hundred femtoseconds of the simulation, collisional energy relaxation from electrons to ions is not important, and the ions gain energy dominantly through acceleration by the space-charge electric field.

Table 2.1 Cluster Parameters for argon and deuterium Clusters

Cluster Material	Initial Ion Density (cm^{-3})	Maximum Ionized state, Z	Initial Electron Density	Mass of Ion (amu)
argon	1.742×10^{22}	Z = 8	$n_e \sim 80\ n_{cr}$	40
deuterium	5.98×10^{22}	Z = 1	$n_e \sim 34\ n_{cr}$	2

The 2D simulations, corresponding to an initially cylindrical cluster, are carried out on a 1024×1024 square mesh of spacing 0.805nm. In most of our simulations, unless otherwise stated, we solve the Poisson equation with open boundary conditions, and particles are allowed to leave the simulation region. Once a particle leaves, its momentum and position are still tracked assuming it responds only to the laser electric field. This is important in calculating the electric dipole moment of the exploding cluster. The distance to the simulation boundary is sufficiently far from the cluster core that only a small fraction of the electrons leave the simulation box for most of the pulse duration.

If the number density of clusters in the irradiated volume is high, energetic ions from neighboring clusters are expected to interact especially towards the end of the pulse when the cluster has expanded significantly. The effect of neighboring clusters alters the evolution of the energy spectrum of ions and electrons. The energy distribution of ions is directly used for determining the fusion neutron yield. In order to incorporate the effect of ions from neighboring clusters on the kinetic energy distribution of ions, we employ periodic boundary conditions to solve the Poisson equation and we allow escaping particles to re-enter the simulation domain. In this case, the size of the simulation box defines the inter-cluster distance. We assume that the clusters are distributed uniformly in the irradiated volume. Then the inter-cluster distance is simply $(n_{cl})^{-1/3}$, where n_{cl} is the number density of clusters. For our simulations parameters (1024×1024 mesh with mesh spacing of 0.805 nm), the inter-cluster distance is 824.32 nm which corresponds to $n_{cl} = 1.78\times10^{12}$ cm^{-3}.

2.3 Effect of Pulse Duration on Resonant Heating

We have done a series of PIC simulations for a range of peak intensities at three different pulse widths for both argon and deuterium. The initial cluster radius was fixed at D_0 = 38nm. The pulse width defined the full width at half maximum of the Gaussian laser pulse envelope. The peak intensity is varied from 1×10^{13} W/cm^2 to 1×10^{16} W/cm^2 with the pulse widths corresponding to FWHM of 100fs, 250fs, and 1ps for argon and 70fs, 100fs and 500fs for deuterium.

In Fig 2.1, we plot the average kinetic energy per electron for cluster electrons (solid) and ions (dotted), and the electrostatic field energy per electron (dashed) in the cluster for D_0=38nm and laser peak intensity of 3×10^{15} W/cm^2 and pulse width of

250fs. Also shown is the laser intensity profile. Initially, the laser electric field pulls out a small fraction of the electrons at the cluster boundary. Accelerated by the electric field in the cluster potential, these escaped electrons absorb energy and the mean electron kinetic energy is increased. As the laser intensity rises, more electrons are pulled out of the cluster and electron excursion length is also increased resulting in stronger heating of the cluster. The mechanism of electron heating is described in detail when we discuss phase space plots later in the chapter.

The charge imbalance created by the extraction of electrons causes an outward directed electric field that accelerates the ions. The electron energy is thus transferred to ions via the electrostatic field energy stored in the space-charge field. The cluster expands due to the coulomb force of the space charge on the cluster ions. Electron extraction and heating decreases later in the pulse when the laser electric field starts falling and the cluster boundary has expanded. This, accompanied by the continued expansion of the cluster core, causes the electron and field energies to fall. Towards the end of the pulse the space charge field energy approaches zero as the expanding ions decrease the charge imbalance. The mean ion energy saturates as most of the electron energy is transferred to the ions and the electrons are no longer extracting energy from the pulse.

Our simulations indicate that there is an intensity threshold for strong heating at which there is a sharp increase in the laser energy coupled to the cluster electrons. This threshold effect is seen clearly in Fig 2.2 that plots the total absorbed energy (sum of electron, ion and electrostatic field energy) per electron at the end of the pulse versus peak laser intensity (scaled to the cluster diameter squared) for different

pulse durations – 100 fs, 250 fs, 500 fs and 1 ps for argon (labeled as 'Ar' in the legend)and 70 fs and 100 fs for deuterium (labeled with a 'D' in the legend). The curves for shorter pulse durations (100 fs, 250 fs for argon and 70 fs, 100 fs for deuterium) exhibit a steep rise in the absorbed energy indicating that there is a critical intensity beyond which the cluster experiences enhanced heating. This threshold intensity is different for different cluster material (argon/deuterium) and laser pulse duration. In reference [53], it was shown for the case of 100 fs pulse duration and argon clusters that the threshold for strong absorption is due to a nonlinear electron transit time resonance. The critical intensity for the onset of this resonance was predicted as the intensity for which energetic electrons take exactly a laser period to transit once through the cluster. The dependence on cluster material and laser pulse duration as seen here is not predicted by the scaling law predicted by Taguchi and Antonsen [53, 54]. In the following paragraphs we will look at electron phase space plots to explore this in greater detail. The threshold-like behavior is less prominent for the longer pulse duration of 500 fs and almost disappears for the even longer pulse width of 1 ps. The absence of a clear threshold for the 1 ps pulse duration results from strong heating of the cluster over a wider range of peak laser intensities and we look at electron phase space plots at three different intensities for 1 ps pulse duration to understand the process of laser to cluster energy for long pulse durations. Further, we note that in all cases the average energy absorbed per electron reaches a saturation value at high intensity, and that the saturation value does not depend monotonically on pulse duration. In particular, for argon cluster, the saturation value for pulse duration of 250 fs exceeds that for both 100 fs and 1 ps pulses. The curve labeled 'Ar-

Circ' is for a series of runs for argon clusters irradiated with circularly polarized laser light of 100 fs pulse duration.

The process of energy absorption by cluster electrons is related to that proposed by Brunel [57] for heating of laser-driven electrons at planar solid-vacuum interface where the electron excursion amplitude is larger than the local density scale length. This is applicable to clusters where the laser pulse accelerates energetic electrons out from the cluster core and drives them back into the shielded cluster. We look at the electron phase space at peak laser intensity of 5×10^{15} W/cm^2, just beyond the threshold for the case of 100 fs pulse duration. Fig 2.3(a) shows a snapshot of this phase space at t = 188.17 fs (the peak of the pulse occurs at 170 fs). Here, the axes are the x coordinate of position and the x component of velocity (v_x) for all electrons in the narrow layer $|y| < \Delta$ along the x-axis, where Δ is the grid size. The high concentration of particles in a band about the center at small v_x represents the core electrons in the cluster. In this region, the laser field is strongly shielded. We note that this core region is roughly 40 nm in size, indicating that the cluster does not expand appreciably before the time of this phase plot. The less dense bunch of electrons at higher magnitudes of velocity corresponds to energetic electrons in the range of 2-10 KeV, which have been pulled out from a thin layer at the cluster surface by the laser electric field. The laser field accelerates these electrons and passing through the cluster they emerge on the other side in phase with the laser field and are further accelerated. The energetic electrons of Fig 2.3(a) take one full laser period to travel once around the cluster to come back to the same position. This matching of electron

transit time to the laser period sets up the resonance condition for irradiating laser pulse of 100fs duration as described by Taguchi and Antonsen [53, 54].

Fig 2.3(b) plots the phase space for a laser pulse of 250 fs FWHM with peak intensity 3×10^{15} W/cm^2 at t = 432.4 fs (the peak of the laser pulse occurs at 430.2 fs). As seen from Fig 2.2, this corresponds to an intensity just beyond the threshold for strong heating and corresponds to 5×10^{15} W/cm^2 for the 100 fs pulse duration. Here, there are two tendrils of energetic electrons, and each bunch moves halfway around the cluster in a laser period. Thus the energetic electron transit time for 250 fs case equals twice the laser period.

Let the number of laser periods required by the hot electron bunch to transit once around the origin of the phase space be defined as N_{res}. Then $N_{res} = 1$ for a 100fs pulse, and $N_{res} = 2$ for a 250fs pulse. In the following paragraph we show that the electron transit time resonances with higher values of N_{res} would lead to a lower intensity threshold.

We assume that the cluster has not expanded appreciably before the onset of strong heating. Phase space plots of Fig 2.3 show that this assumption holds reasonably well for those cases. For enhanced cluster heating characterized by an electron transit time resonance of order N_{res}, we can write the condition for strong heating as

$$\left(\frac{2D_0}{v_{cluster}}\right) = N_{res}\left(\frac{2\pi}{\omega}\right) \qquad (2.1),$$

where D_0 is the initial cluster diameter, $v_{cluster}$ is the average velocity of an electron transiting the cluster, N_{res} is the order of resonance at the time of strong heating and ω

is frequency of the laser pulse. For the case of electron heating at a planar-solid interface considered by Brunel [57], the peak velocity of electrons driven into the planar surface was given as $\upsilon_{plane} = 2eE_s / m_e\omega$, where E_s is the laser field at the surface, and the factor of 2 is due to the effective field boost provided by the space charge. The space charge field acts opposite the laser electric field during extraction, but adds to it when electrons are accelerated back into the bulk plasma. For our case of laser heating in clusters for the 2D geometry, there is an additional factor of 2 due to the dielectric focusing of the electric field lines by the cylindrical cluster. The extracted electrons, however, do not all have the same energy nor are they at the same phase with respect to the laser field resulting in the typical velocity of electrons transiting the cluster being lower than the peak velocity. We assume it to be half the peak velocity, i.e. $v_{cluster} = 0.5(2v_{plane}) = v_{plane}$. Substituting this in Eqn. (2.1) we get the scaled critical intensity for strong absorption as,

$$\frac{I_0}{D^2{}_0} = \frac{c}{8\pi}\left(\frac{m_e\omega^2}{2\pi e}\right)^2 \frac{1}{N^2{}_{res}} \qquad (2.2).$$

The threshold intensity is inversely proportional to the order of resonance as seen in Eqn.(2.2). Thus the intensity threshold for 250 fs pulse duration ($N_{res} = 2$) is lower than that for 100 fs case ($N_{res} = 1$). It is important to note that the cluster does undergo higher N_{res} stages even for the case of 100 fs FWHM and peak intensity 5×10^{15} W/cm^2 earlier in the pulse [53], but the cluster does not absorb significant energy at these higher resonances. Because of the strong shielding effect of the core electrons, energetic electrons gain energy only when they are outside the cluster. The higher the order of the resonance, the smaller the fraction of time an electron is

heated. Consequently, for strong absorption at higher N_{res} the cluster needs to spend longer time at the resonance. This is possible only with longer pulse durations where the temporal variation of the laser electric field is lower. For the 250fs laser pulse, the cluster spends a significant time in a resonance stage characterized by N_{res} =2 and experiences enhanced laser pulse energy absorption at the lower peak intensity of 3×10^{15} W/cm^2. For 100fs pulse width the laser pulse envelope varies more quickly and the peak laser intensity needs to be as high as 4.7×10^{15} W/cm^2 at which the cluster electrons gain energy with every laser cycle (N_{res} =1) and experience strong heating.

Fig 2.4 plots similar phase space plots for deuterium clusters for laser pulse of (a) 100 fs FWHM, 3×10^{15} W/cm^2 peak intensity at t = 204 fs, and (b) 70 fs FWHM, 5×10^{15} W/cm^2 peak intensity at t = 148.9 fs. We note that for the 100 fs case, there are two bunches of energetic electrons indicating that N_{res} =2, while N_{res} =1 for the 70 fs case. The intensity threshold is accordingly lower for laser pulse width of 100fs FWHM.

Another feature observed in Fig 2.2 is the decreased prominence of the intensity threshold for longer laser pulse durations (500 fs and 1 ps runs). As the pulse duration is increased the manner of energy absorption by the cluster changes significantly. This is seen in Fig 2.5 that plots (a) the total energy absorbed per cluster electron versus time and (b) root mean squared radius (RMS) of the cluster ions versus time for the peak laser intensities and pulse durations of (5×10^{15} W/cm^2, 100 fs), (3×10^{15} W/cm^2, 250 fs), and (5×10^{14} W/cm^2, 1 ps). These correspond to the intensities beyond which the total energy absorbed saturates for the particular pulse

length. For the 100 fs and 250 fs pulse lengths these peak intensities are just above the threshold for strong heating. The plotted RMS radius of the cluster ions is normalized to the initial RMS value and is a measure of cluster expansion. In either figure, time (horizontal axis) is normalized to the pulse length. The shape of the pulse envelope is shown as the thin dotted line in Fig 2.5(a). We note that for 100 and 250 fs cases energy absorption by the cluster takes place later in the pulse with fastest absorption taking place just after the peak has passed. This is due to enhanced heating with the onset of the transit time resonance. For the case of 1 ps pulse length, however, the cluster starts absorbing energy much earlier in the pulse when the intensity is low. In addition, Fig 2.5(b) shows that the cluster starts expanding much earlier in the pulse for longer pulse lengths. Specifically the RMS radius of cluster ions increases to roughly 20 times the initial value for the case of 1 ps pulse length and to about 1.5 times the initial value for 250 fs, while it hardly changes for the shorted pulse length of 100 fs. In the following paragraph we look at electron phase space plots for the 1 ps case.

Fig 2.6(a) shows the phase space plot at t = 1720 fs (peak of pulse is at 1700 fs) for a cluster irradiated with a laser pulse of 1 ps FWHM and peak intensity 5×10^{14}W/cm^2. In the phase space plot we can make out 9 distinct bunches of energetic electrons. In other words, N_{res} =9 for the conditions of Fig 2.6(a). In addition, we note that the cluster core is significantly enlarged. This is because the cluster absorbed energy and expanded earlier in the pulse when the intensity was lower. In Fig 2.6(b) and (c), we look at phase space plots at lower peak intensities 1×10^{14}W/cm^2 (7b) and 5×10^{13}W/cm^2 (7c). The basic characteristics of these phase

spaces are similar to the higher intensity case of 5×10^{14}W/cm^2 but show even higher orders of resonances of N_{res} = 10, and N_{res} = 16 respectively. The phase space study shows that at pulse length of 1 ps, the cluster can spend much longer times at each resonance stage leading to significant energy absorption at very high orders of resonance and lower peak intensities. As the peak intensity increases it supports lower orders of resonance and absorbs energy more efficiently, finally leading to saturation in energy absorbed beyond 5×10^{14}W/cm^2. Absorption of energy at a wide range of N_{res} leads to gradual increase in energy absorbed with increasing peak intensity as compared to the 100 fs case where there is a sharp threshold, marked by a transition to the N_{res} = 1 state.

Finally in Fig 2.2 we note that the intensity threshold for circularly polarized laser pulse is higher than that for the linearly polarized pulse. Fig 2.2 shows that the intensity threshold for circular polarization is just below 1×10^{16} W/cm^2 while the corresponding point for the linear polarization case is 5×10^{15} W/cm^2. For the same peak laser intensity, the peak electric field in any one direction for circularly polarized case is $1/\sqrt{2}$ times the linearly polarized field in the polarization direction. Thus for the circularly polarized pulse the threshold peak laser intensity needs to be twice that for linearly polarized case for the transit time resonance of N_{res} = 1.

2.4 Ion and Electron Kinetic Energy Distributions

Fig 2.7 plots (a) the electron kinetic energy spectra, $F_e(E,t)$, and (b) the ion kinetic energy spectra, $F_i(E,t)$ for an irradiated argon cluster. The product $(F_{e,i}dE)$ represents the fraction of electrons (ions) in the interval dE at a given kinetic energy E. The three spectra labeled (a-c) in each plot correspond to laser pulses of equal

energy for the following pulse width and peak intensity combinations: (a) 100 fs, 1×10^{16} W/cm^2; (b) 250 fs, 4×10^{15} W/cm^2; (c) 1000 fs, 1×10^{15} W/cm^2. Each of these cases considered is above the threshold for strong heating. A quasi-mono-energetic peak characterizes the energy distribution of the emerging ions. As electrons are extracted from the cluster by the laser electric field they form a halo of energetic electrons around the cluster. The ions gain energy as they are pulled out by this space charge around the cluster. Initially this leads to an ion energy distribution that is monotonic in energy and radial distance with the highest energy ions also being at the largest radial distance from the center of the cluster. As the ions and electrons expand, the electrostatic potential changes with time. This results in ions that have been accelerated later gaining more energy and over-taking the ions accelerated earlier. The beam-like distribution is associated with this overtaking process that leads to an increase in the population of ions at energy slightly below the maximum energy.

Both electron and ion kinetic energy distributions show an increase in the energy as the pulse width is increased from 100fs to 250fs and then the energy falls as the pulse width is further increased to 1ps. This trend follows that of the average energy absorbed in the saturated regime depicted in Figure 3. The effect is more dramatic for ions with the peak ion energy varying from about 800 KeV for laser FWHM of 100 fs (a) to 1400 KeV for 250 fs FWHM (b) and finally falling to 250 KeV for 1000 fs (c). To explain this we note that for pulse duration of 100 fs, the cluster does not disintegrate completely by the time the pulse has passed over it. Thus if the pulse duration is increased from 100 fs the cluster can absorb heat for a longer period of time before it disintegrates. This leads to higher absorption of energy by the

cluster electrons and the corresponding higher ion energies. However, as the pulse duration is increased further the cluster starts disintegrating earlier in the pulse. Once the cluster has disintegrated and the electrons respond as if they were free (that is, the self-field of the cluster is unimportant) heating stops. This leads to the fall in the peak electron and ion energies as observed for the 1 ps case. This also explains the higher saturation value of the total energy absorbed by the cluster for the 250 fs pulse duration as compared to the 100 fs and 1 ps pulses.

As a cluster expands it eventually encounters particles from neighboring clusters. The greater the number density of clusters, the sooner this would happen. Generally when the expanding clusters encounter one another the result is that the accelerating potential resulting due to the expanding electrons is driven to zero and evolution of the distribution functions ceases. Using periodic boundary conditions in the simulations allows for such inter-cluster ion and electron interaction to take place. Fig 2.8 plots the ion energy distribution functions, $f_i(E,t)$ versus energy for a 38nm deuterium cluster. The curves labeled (a)-(e) are obtained using periodic boundary conditions peak laser intensities of 1×10^{15} W/cm^2, 3×10^{15} W/cm^2, 1×10^{16} W/cm^2, 5×10^{16} W/cm^{2}and 1×10^{17} W/cm^2 respectively. As in the case of argon clusters, we see an ion distribution function dominated by high-energy ions for intensities above the threshold for strong heating at 3×10^{15} W/cm^2. The spectrum for the below-threshold peak laser intensity of 1×10^{15} W/cm^2, marked as (a), does not have this character. The space charge field for such low laser intensities is not enough to accelerate a large number of ions to the boundary of the electron cloud surrounding the cluster. For intensities much higher than the threshold intensity the distribution

function actually increases with increasing energy, reaches a maximum and then finally falls off. Also, the maximum ion energy is seen to increase monotonically with the peak laser intensity. In the following section we show how this pronounced dependence of the ion energy spectrum on the peak laser intensity would impact the fusion yields for laser-irradiated clusters.

2.5 Nuclear Fusion and Neutron Yield

Energetic ions from exploding deuterium clusters can undergo thermonuclear fusion producing neutrons as represented by the reaction

$$D + D \xrightarrow[50\%]{} He^3(0.82\ MeV) + n\ (2.45\ MeV) \qquad (2.3).$$

To calculate the rate of fusion reactions we assume that the ions at all energies are distributed uniformly in space. This is a reasonable assumption for periodic boundary conditions towards the end of the pulse when the energetic ions have expanded to beyond the simulation boundary. There is also the possibility of neutron production via two-step process such as

$$\begin{aligned} D + D &\xrightarrow[50\%]{} T + p \\ D + T &\xrightarrow[50\%]{} He^4 + n \end{aligned} \qquad (2.4),$$

but for the parameter ranges under consideration the total yield of products from the first reaction in Eqn. (2.4) is not large enough to necessitate the consideration of follow-up reaction. Hence we only consider Eqn. (2.3) here for calculating neutron yield. The number of fusion reaction per second per unit volume is then given as

$$R(t) = \frac{1}{2} n_{av}{}^2 \int dE \int dE'\, f_i(E,t) f_i(E',t) \left\langle \sigma\left(E_{rel}\right) \left| \mathbf{v} - \mathbf{v}' \right| \right\rangle_\theta \qquad (2.5),$$

where n_{av} is the average density of ions over the simulation region, $f_i(E,t)$ is the

kinetic energy distribution of ions given by , σ is the reaction cross-section and **v** is the ion velocity such that $m_i|\mathbf{v}|^2 = 2E$, m_i being the ion mass. The reaction cross-section σ is expressed as a function of the relative energy of the interacting ions, $E_{rel} = m_i|\mathbf{v}-\mathbf{v}'|^2/2$ where **v** and **v'** are the velocities of the interacting ions. The angled brackets denote an averaging over all possible angles θ, assuming that the ion distribution is isotropic. Equation (2.6) below gives the reaction cross-section [69, 70] (in cm^2)

$$\sigma(E_{rel}) = \frac{A_5 + [\{A_4 - A_3(E_{rel})\} + 1]^{-1} A_2}{(E_{rel})[\exp\{A_4(E_{rel})^{-1/2}\} - 1]} \times 10^{-24} \qquad (2.6),$$

where (E_{rel}) is in keV. The Duane coefficients A_j have the values A_1=47.88, A_2=482, $A_3=3.08\times10^{-4}$, A_4=1.177, and A_5=0 for the particular reaction in Eqn. (2.3).

In order to calculate the yield of fusion neutrons we consider a cylindrical volume, $V = (2\pi w_0)(2z_r)$ where w_0 is the spot size of the laser beam and z_r is the Rayleigh length associated with that spot size. We assume that the interaction time for ions is limited by the average time required by the higher energy ion to exit this volume. The total neutron yield can then be calculated as

$$NY = \frac{1}{2} n_{av}{}^2 V D_{avg} \int dE \int dE' f_i(E,t) f_i(E',t) \left\langle \sigma\left(E_{rel}\right) |\mathbf{v}-\mathbf{v}'| \right\rangle_\theta \frac{1}{\max\left(|\mathbf{v}|,|\mathbf{v}'|\right)} \qquad (2.7),$$

where D_{avg} is the average distance from the center to the edge of the volume under consideration.

Fig 2.9 plots reaction rate per unit volume at t = 300 fs (solid) and total neutron yield (dotted) for fusion of energetic ions from exploding laser–irradiated deuterium clusters with pulse peak intensities ranging from 1×10^{15} W/cm^2 to 1×10^{17}

W/cm^2. The threshold intensity for this set of runs was at 3×10^{15} W/cm^2. The plot shows a sharp rise in the reaction rate as the intensity crosses the non-linear resonance threshold. This is due to the increase in the number of high-energy ions as the intensity crosses the threshold. For intensities much above the threshold, the fusion rate and neutron yield both saturate as the cluster disintegrates earlier in the pulse.

It should be noted that in actual experiments effects such size distribution of clusters, absorption and self-focusing of the pulse, and spatial distribution of energetic ions would play a significant role in determining the total neutron yield. Thus the neutron yield in an experiment might be different from that based on the fusion reaction rate calculated here.

2.6 Summary and Conclusions

We describe the effect of laser pulse duration on resonant heating of laser-irradiated clusters. The clusters absorb heat via a non-linear resonance mechanism where electrons are first accelerated out from the cluster and then driven back into it by the combined effects of the laser field and the electrostatic field produced by the laser-driven charge separation. The energetic electrons then pass through the cluster and emerge on the other side. If they emerge in phase with the laser field, there is resonant heating, and the cluster quickly absorbs energy. The onset of this 'transit time' resonance depends on the ratio of laser intensity to cluster size for a given pulse duration. Our simulations of argon and deuterium clusters show that as the pulse duration is increased the cluster absorbs energy at higher order resonances with the electron transit time equaling more than one laser period. This increase in the order of the resonance leads to the lowering of the intensity threshold for strong heating. As

the pulse length is increased further our simulations how that the threshold becomes less dramatic and almost disappears for 1 ps pulse length. This is because at increased pulse lengths, even for low peak intensities the cluster can absorb significant energy due to longer times in high order resonant states. The calculation for predicting intensity threshold for a given cluster diameter as derived in reference [53] has been generalized to take the higher order resonances into account. Our generalized formulation predicts intensity thresholds that are inversely proportional to the square of the order of resonance during strong heating. However, the predicted threshold intensities increasingly deviate from the values obtained from simulations as the pulse width is increased to 1000 fs. This is due to cluster expansion earlier in the pulse for longer pulse widths, an effect that was not taken into account for calculating the predicted intensity thresholds.

Our results indicate a strong pulse duration dependence of the kinetic energy distribution of the cluster ions and electrons with the maximum ion energy going up from 800 keV to 1.4 MeV as the pulse width is increased from 100fs to 250fs, but then falling off to 250 keV as the pulse width is increased further to 1000 fs. The pulse energy was kept constant for this set of runs. This is of consequence for possible applications in laser-based accelerators and for fusion neutron production from clusters.

We have investigated the fusion reaction rate and neutron yield for deuterium clusters for a 100 fs FWHM pulse of peak intensities ranging from 10^{15}-10^{17} W/cm^2. We find that there is a dramatic increase in the reaction rate and neutron yield as the intensity crosses the threshold for strong heating at 3×10^{15} W/cm^2. The reaction rate

saturates beyond the peak intensity of 5×10^{15} W/cm^{2}as the intensity is increased to 1×10^{17} W/cm^2.

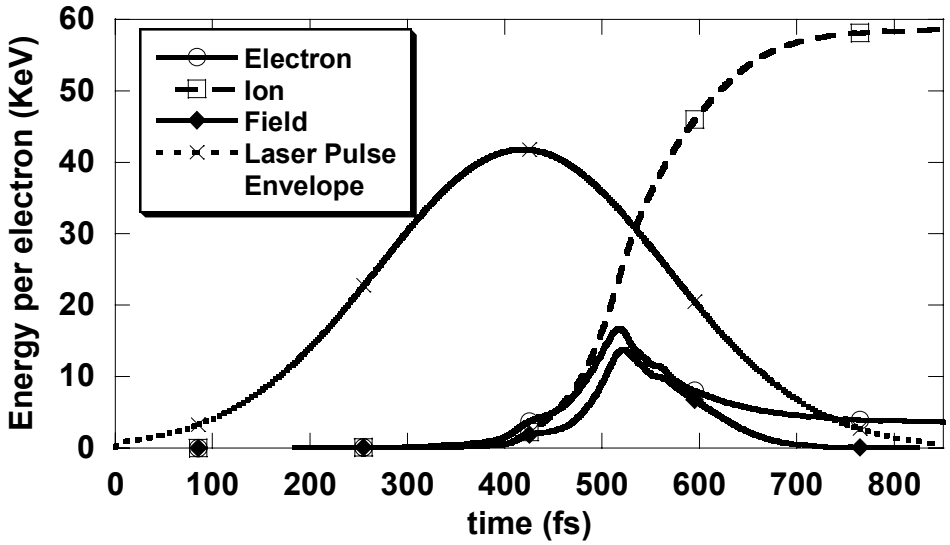

Fig 2.1 Electron (solid line with circles), Ion (dashed line with squares) and Electrostatic Field Energy (solid line with diamonds) per cluster electron as a function of time for an argon cluster with D_0=38nm and laser pulse of peak intensity 3×10^{15} W/cm^2 and FWHM of 250fs. The laser field profile is shown on the same time axis by the dotted line with crosses. The applied field accelerates the electrons, creating a charge separation that in turn accelerates the ions.

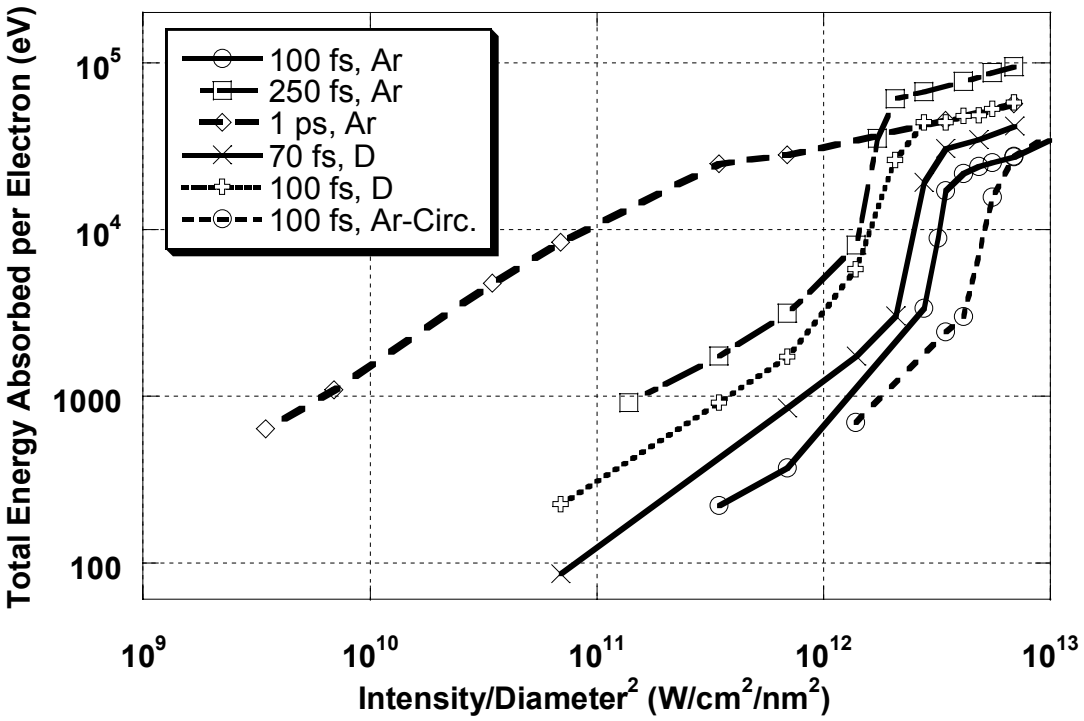

Fig 2.2 Total energy absorbed by the cluster (sum of electron, ion and electrostatic field energies) per cluster electron versus the laser intensity for a range of pulse durations for argon and deuterium clusters. The curves are labeled in the legend by the pulse duration for that curve and as 'Ar' for argon and 'D' for deuterium. The curve labeled '100fs, Ar-Circ' is for a circularly polarized laser pulse of duration 100 fs. All other curves are for linearly polarized laser pulse. The laser intensity has been normalized to the square of the initial diameter of the cluster. Note the dramatic intensity threshold for strong energy absorption for both argon and deuterium at lower pulse durations. The intensity threshold is lowered as the pulse length is increased, and becomes less prominent for very long pulse lengths.

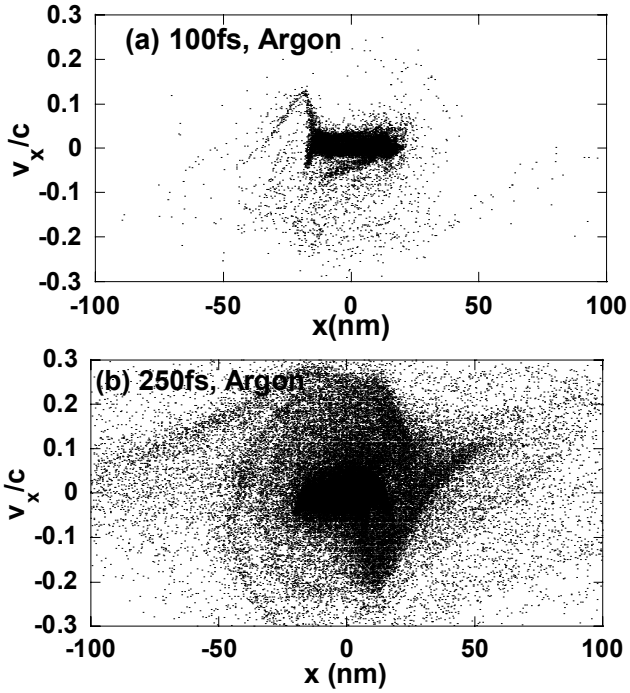

Fig 2.3 Phase space (x-v_x) plots for electrons near the x-axis for argon cluster. The two plots correspond to peak laser intensity and pulse length of (a) 5×10^{15} W/cm^2, 100 fs and (b) 5×10^{15} W/cm^2, 250 fs. Note that $N_{res} = 1$ for (a) and $N_{res} = 2$ for (b). Increase in the order of resonance leads to lowering of intensity threshold.

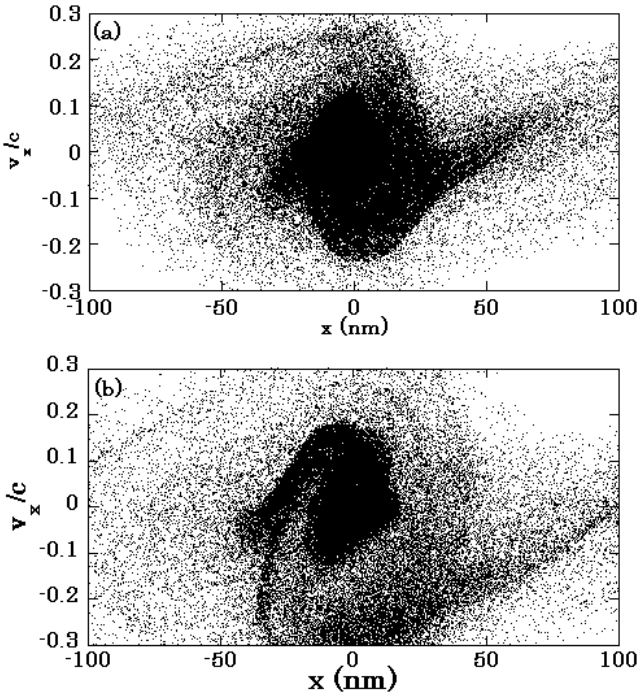

Fig 2.4 Phase space (x-v_x) for electrons near the x-axis for deuterium cluster for (a) 100fs FWHM, 3×10^{15} W/cm^2 peak intensity at t = 204.8 fs and (b) 70 fs FWHM, 5×10^{15} W/cm^2 peak intensity at t = 148.9 fs. The plots show that N_{res}=2 for (a) and N_{res}=1 for (b).

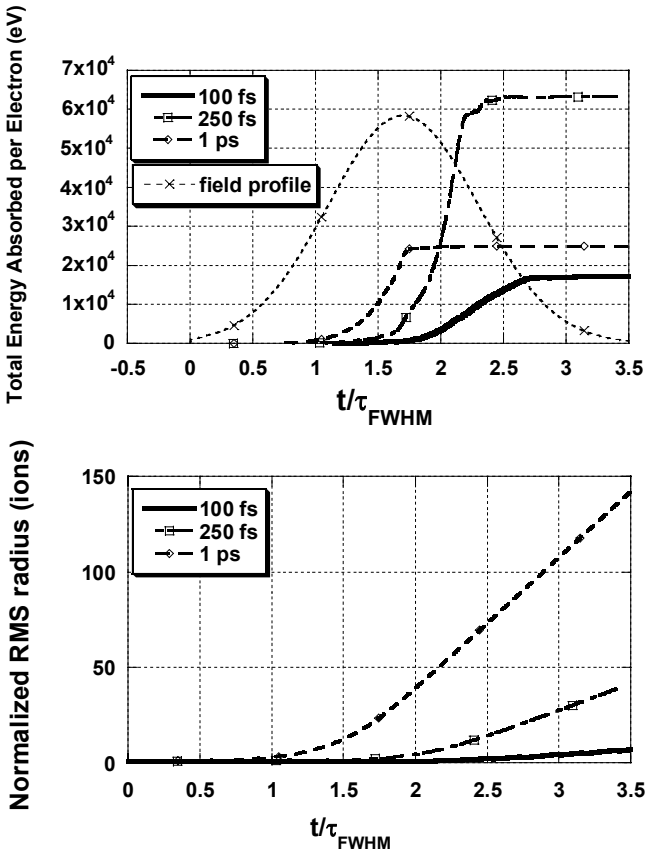

Fig 2.5 (a) Total energy Absorbed per Electron and (b) Root mean squared radius of cluster ions for 100fs, 5×10^{15} W/cm^2 (solid), 250fs, 3×10^{15} W/cm^2 (dashed), and 1000fs, 5×10^{14} W/cm^2 (dash-dot). For the case of 1 ps pulse length, the cluster absorbs energy and expands much earlier in the pulse when the electric field is much below the peak.

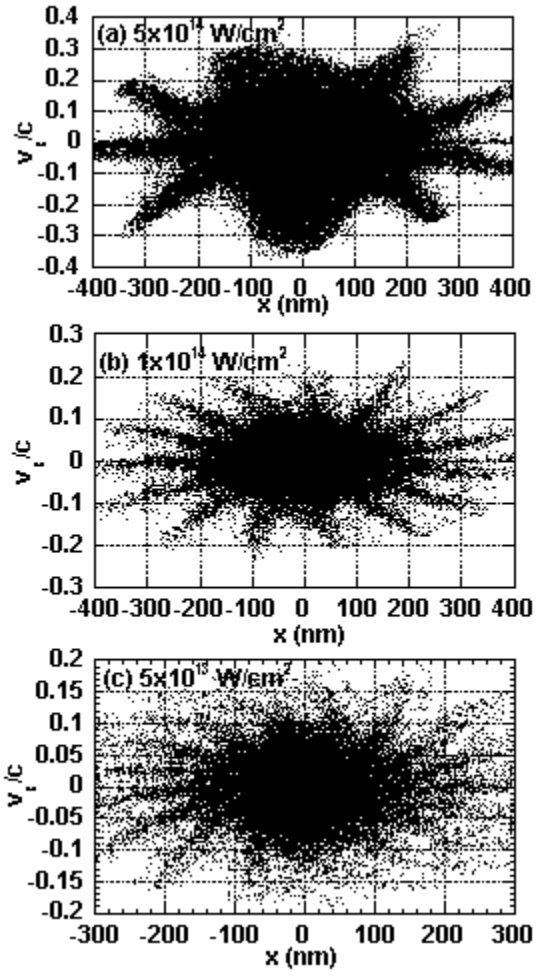

Fig 2.6 Phase space (x-v_x) for electrons near the x-axis for argon cluster for 1 ps FWHM and peak intensity of (a) 5×10^{14} W/cm^2, (b) 1×10^{14} W/cm^2 and (c) 5×10^{13} W/cm^2 at t = 1720 fs. The plots show that N_{res}.= 9, 15, and 19 for (a), (b) and (c) respectively.

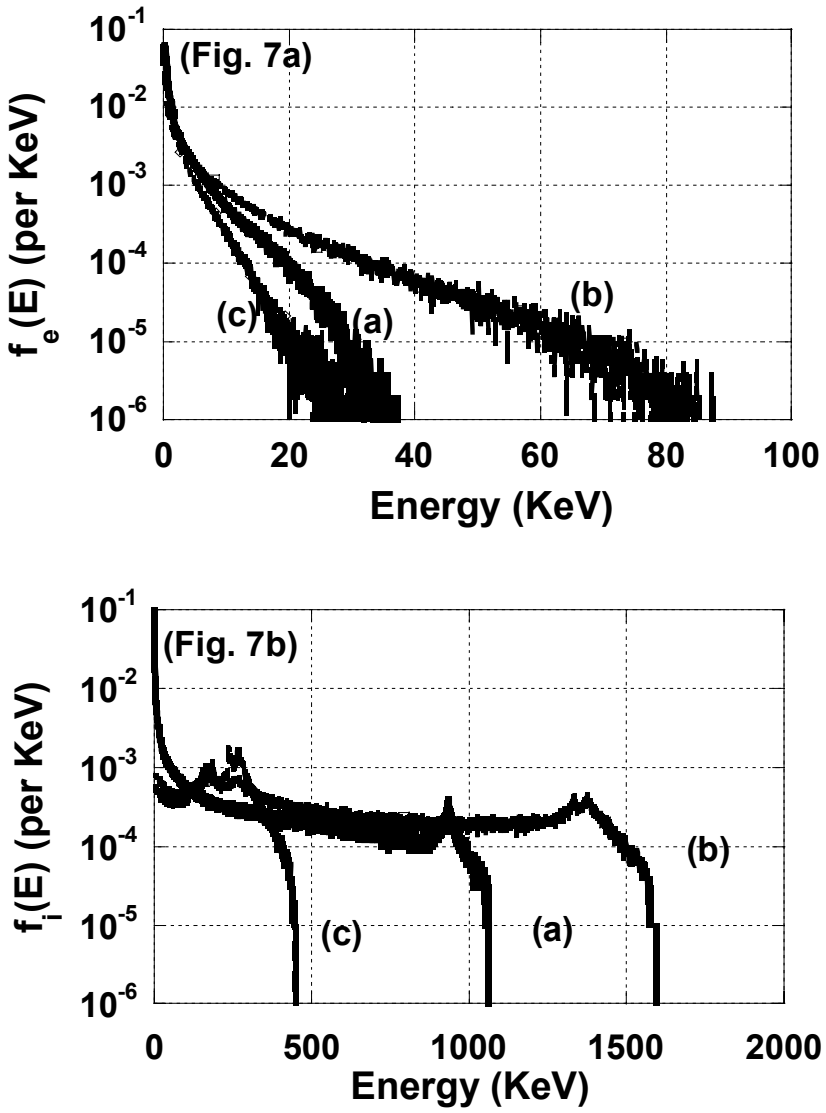

Fig 2.7 Electron(7a) and ion (7b) kinetic energy distribution functions for (a) 100fs, 1×10^{16} W/cm^2 , (b) 250fs, 4×10^{15} W/cm^2, and (c) 1ps, 1×10^{15} W/cm^2. A quasimonoenergetic peak of ions dominates the ion distribution function. The energy at which this peak occurs is pulse duration dependent. For both electron and ions, the distribution functions show an increase in energy as the pulse length is increased from 100 fs to 250 fs, but in either case the energy falls down as the pulse length is further increased to 1 ps.

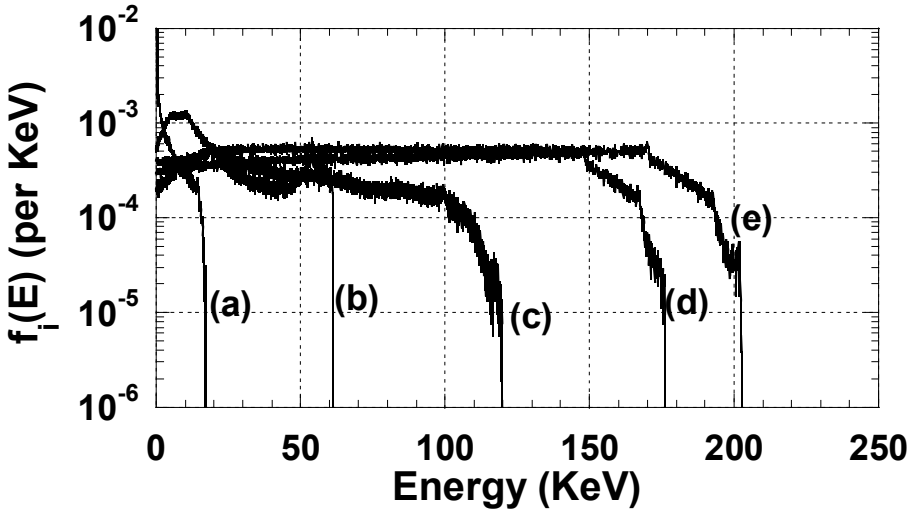

Fig 2.8 Ion kinetic energy distribution functions under periodic boundary conditions for deuterium ions of initial diameter 38nm irradiated with laser pulses of 100fs duration and peak intensities of (a) 1×10^{15} W/cm^2, (b) 3×10^{15} W/cm^2, (c) 1×10^{16} W/cm^2, (d) 5×10^{16} W/cm^2, and (e) 1×10^{17} W/cm^2.

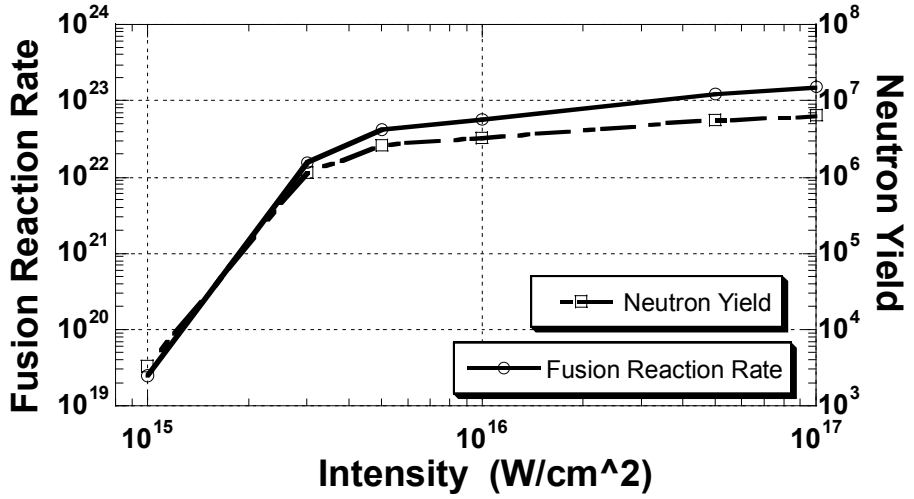

Fig 2.9 Fusion reaction rate per unit volume (left vertical axis) and total neutron yield (right vertical axis) as a function of peak laser intensity for deuterium clusters with D_0 = 38nm.

3 Propagation of Intense Short Laser Pulses in a Gas of Atomic Clusters

3.1 Introduction

Intense laser irradiated gases of atomic clusters act as a unique non-linear optical medium [3]. Experiments on the propagation of laser pulses through clustered gases reveal many unique properties such as self-guiding [17], strong laser pulse absorption [2] and pulse spectrum shifts [37] that are different from similar laser pulses propagating in tenuous gases. When irradiated by a laser pulse, each individual cluster in the ensemble absorbs laser pulse energy and explodes and in the process the effective optical properties of the clustered gas evolve. Theoretical modeling and simulation tools are necessary in order to attain a better understanding and control of this process. While considerable effort has gone into modeling the interaction of an individual cluster with an irradiating laser pulse, studies on effects of laser pulse propagation have been limited and mostly restricted to specific aspects like self-focusing [60] [71] and phase matching [39]. In this chapter we present a fully self-consistent model for studying the propagation of a laser pulse through a gas of exploding clusters and study the experimentally observed effects [72]. The material presented in this Chapter was published as reference [72].

The cluster parameter that directly relates to laser propagation is the individual cluster polarizability γ, defined by the relation $\hat{\mathbf{p}} = \gamma \hat{\mathbf{E}}_{\mathrm{L}}$ where $\mathbf{p}(\mathrm{t}) = \mathrm{Re}\{\hat{\mathbf{p}} e^{-i\omega t}\}$ is the electric dipole moment of the cluster and $\mathbf{E}_{\mathrm{L}}(t) = \mathrm{Re}\{\hat{\mathbf{E}}_{\mathrm{L}} e^{-i\omega t}\}$ is the laser electric field whose frequency is ω. The

temporal evolution of γ determines the time variation of the effective dielectric constant of the ensemble of clusters given as

$$\left(\varepsilon_{eff}\right)_{medium} = 1 + 4\pi n_c \gamma \,, \tag{3.1}$$

where n_c is the number density of clusters. In an experiment on the time-resolved explosion dynamics of laser-irradiated clusters, Kim et al. [73] measured the complex cluster polarizability. It is of significance to use an experimentally consistent model of the cluster polarizability γ for any realistic simulation of pulse propagation through cluster plasma. In addition, the model for individual cluster polarizability needs to be computationally simple for propagation studies would require simulating tens of thousands of clusters.

One of the first models of cluster expansion that enables the calculation of polarizability was given by Ditmire [51]. This model treats the cluster as a spherical ball of uniform density throughout the interaction process. Though it has been very useful in explaining many aspects of cluster expansion like high ionization levels, generation of energetic ions, and resonant absorption, the model has drawbacks in that it predicts strong absorption during time intervals much shorter than those measured in experimental studies [66, 74]. Milchberg [52] proposed the fully hydrodynamic model that allows for temperature and density gradients within the cluster. This gives results of cluster dynamics consistent with the experiments measuring the complex transient polarizability of clusters [73]. The polarizability results from the hydrocode are further supported by experiments on scattering and absorption of intense laser pulses in clustered gas [2]. This model, however, is computationally intense and thus unsuitable for studies of pulse propagation where

effectively many clusters must be simulated. Also, fluid models are not expected to be appropriate at intensities of irradiation that are high enough to create a population of energetic electrons. Alternate to the fluid approach are the kinetic models that treat electrons and ions as particles [53, 55, 56, 75]. The particle model can include the effects of energetic particles on the polarizability. However, it is even more computationally intense than the fluid models and the predictions for the cluster polarizability coming from kinetic models have not been fully explored.

We propose a model of cluster expansion that retains the simplifying assumption of a uniform density profile within the cluster, but with modified cluster parameters. Our model generates a temporal polarizability profile consistent with the hydrodynamic model without sacrificing computational speed. This is then coupled to a Gaussian description of the laser pulse. The underlying assumption in our model is that the dominant non-linearity is the intensity dependent rate of expansion of the cluster radius [76]. We assume the electrons respond linearly to the laser field. Energy is absorbed by the cluster due to electron-ion collisions. The heated electrons cause the cluster to expand on a time scale determined by the ion mass. The quasi-linear modification of the cluster profile and radius then changes the linear response of the electrons. Thus we can think of the non-linearity as occurring through the ion motion. This is in contrast to alternative models [58, 60, 77] that emphasize the direct non-linear response of the electrons in the strong laser fields.

Finally we note that above a threshold intensity the electron motion becomes highly non-linear and there is strong production of energetic electrons. The model

presented here is meant to apply for intensities below this threshold where the electron distribution remains thermal.

In the next section we present in detail the equations and assumptions used for simulating the cluster dynamics. Section 3.3 describes the modeling of the laser pulse and the pulse propagation equations. Equilibrium and stability of the pulse parameters are considered in Section 3.4. The results of numerical simulation are presented in Section 3.5.

3.2 Cluster Model

Perhaps the most basic model for the heating and expansion of atomic clusters in the presence of intense fields is the uniform density model given by Ditmire *et al.* [51]. In this model, the clusters are treated as uniform dielectric spheres with no temperature or density gradients inside the cluster. The dynamical variables which describe the cluster are the (uniform) electron temperature, electron density and ion density, and radius of the cluster $a(t)$.

If the cluster is much smaller than a laser wavelength, the electric field in and around the cluster can be determined in the electrostatic approximation. Inside the cluster the electric field is uniform and is given by $\mathbf{E}_{\mathrm{i}}(t) = \mathrm{Re}\{\hat{\mathbf{E}}_{\mathrm{i}} e^{-i\omega t}\}$ where

$$\hat{\mathbf{E}}_{\mathrm{i}} = \frac{3}{\varepsilon_{cluster} + 2}\hat{\mathbf{E}}_{\mathrm{L}}, \tag{3.2}$$

and $\mathbf{E}_{\mathrm{L}}(t) = \mathrm{Re}\{\hat{\mathbf{E}}_{\mathrm{L}} e^{-i\omega t}\}$ is the laser electric field. The dielectric constant inside the cluster, $\varepsilon_{cluster}$, will be determined mainly by the response of the free electrons and is given by the Drude model [78],

$$\varepsilon_{cluster} = 1 - \frac{\omega_p^{\,2}}{\omega^2(1 + i\nu/\omega)}, \tag{3.3}$$

where $\omega_p^2 = 4\pi n_e e^2/m_e$ is the plasma frequency, e and m_e are the electron charge and mass and ν is the electron-ion collision frequency. For large values of $\varepsilon_{cluster}$ the electric field is shielded from inside of the cluster i.e. $\left|\hat{\mathbf{E}}_{\mathrm{i}}\right| \ll \left|\hat{\mathbf{E}}_{\mathrm{L}}\right|$. An important quantity in determining the evolution of the laser pulse is the response of the cluster to the laser field, which is characterized by the cluster complex polarizability, γ. This is defined by the relation $\hat{\mathbf{p}} = \gamma \hat{\mathbf{E}}_{\mathrm{L}}$ where $\mathbf{p}(\mathrm{t}) = \mathrm{Re}\{\hat{\mathbf{p}} e^{-i\omega t}\}$ is the electric dipole moment of the cluster. For a spherical cluster of uniform dielectric constant, $\varepsilon_{cluster}$, the polarizability of the cluster is

$$\gamma = \frac{\varepsilon_{\mathrm{cluster}} - 1}{\varepsilon_{\mathrm{cluster}} + 2} a^3, \tag{3.4}$$

where a is the radius of the cluster.

To apply Eq. (3.3) and (3.4), a model for the evolution of the electron temperature and density in the cluster and the radius of the cluster is required. The free electron density in the cluster evolves due to several processes [52]. Initially free electrons are produced by direct ionization of the cluster atoms in the presence of the laser field. Further ionization occurs via electron-ion inelastic collisions, facilitated by the high density inside the cluster. The free electrons, thus produced, absorb laser-energy primarily through collisional inverse bremsstrahlung process. Finally, the density decreases as the cluster expands. In our version of the model, these processes are treated as follows. We will assume that ionization occurs instantaneously once the intensity exceeds a certain threshold. At that time the cluster atoms will be ionized to

a specific state Z. The electron and ion densities are then taken to be $n_e = Zn_i = ZN_a/V$ where N_a is the number of atoms and $V = 4\pi a^3/3$ is the volume of the cluster.

The expansion of the cluster is due to the thermal energy of the heated electrons and is restrained by the inertia of the ions. If the cluster remains quasi-neutral the evolution of the cluster radius can be determined by balancing the rate of increase of ion kinetic energy, $K_i = (2\pi/5)m_i n_i a^3 \dot{a}^2$ against the rate at which work is done by the electron pressure in expanding the cluster,

$$\frac{dK_i}{dt} = P_e \frac{dV}{dt} = P_e 4\pi a^2 \frac{da}{dt}, \tag{3.5}$$

where $P_e(t)$ is the electron pressure and m_i is the ion mass. The expansion of the cluster thus obeys

$$\frac{d^2 a}{dt^2} = 5\frac{P_e}{m_i n_i a}. \tag{3.6}$$

The electron pressure is obtained by balancing the rate of increase of internal energy of electrons against the sources and sinks of electron energy,

$$\frac{d}{dt}\left(\frac{3}{2}VP_e\right) = -P_e \frac{dV}{dt} + \dot{U}V, \tag{3.7}$$

where $\dot{U}$ is the rate of energy absorption per unit volume, given by,

$$\dot{U} = \frac{9}{8\pi}\frac{\mathrm{Im}(\varepsilon)}{|\varepsilon + 2|^2}\omega\left|\hat{\mathbf{E}}_{\mathrm{L}}^2\right|. \tag{3.8}$$

The model system (3.5)-(3.8) is based on the assumption that the density and temperature profiles remain flat within the cluster ($r \langle a$). This is not true even if one adopts a fluid model. Recent one-dimensional fluid simulations [52] have shown that the density profile develops a low-density pedestal, which has a significant effect on

the laser electric field and the rate of energy absorption. Further, if one adopts a kinetic picture it is found that there is generation of energetic electrons that are outside the description of the fluid model [53]. In spite of these shortcomings, the simplicity of the uniform density model makes it attractive for plasma propagation studies, provided it can replicate the dynamic behavior of the cluster polarizability.

To use the model we adjust parameters so that the time dependence of the polarizability matches that of calculations obtained from the fluid code of reference [52] These results for polarizability have also been compared favorably with experimental results [73]. The parameters we adjust are the ion mass and the dependence of the collision frequency on temperature and density. In particular, we assign a mass of 3 atomic units for the ions in the cluster as opposed to the expected 40 amu of normal argon ions. The modified collision frequency is given as

$$\nu/\omega = \frac{15}{T_e^{1/4}}, \tag{3.9}$$

where T_e is the electron temperature in electron Volts. The electron temperature is calculated assuming the electrons to behave as an ideal gas with $P_e = n_e T_e$. These two modifications attempt to rectify shortcomings of the uniform density description, as we now describe. From (3.4) we note that if $\varepsilon_{cluster} \gg 1$, then $\gamma \approx a^3$. Thus in the uniform density model the polarizability is real and determined primarily by the cluster radius during the initial expansion. The fluid and the particle simulations show a more complicated picture with the polarizability depending sensitively on the shape of the density profile near the critical surface. In the hydro-model the cluster heating and expansion are primarily determined by the dynamics of the thin critical density layer, as opposed to the uniform density model where the whole cluster comes to

resonance at the same time. One could thus argue, that the evolution of the cluster as a uniform dielectric sphere but with reduced mass captures this effect, allowing the cluster to expand more rapidly. This has the effect of allowing the real part of polarizability to increase more rapidly in time, thus giving results comparable to the hydrocode.

Adjusting the temperature and density dependence of the collision rate also affects the imaginary part of the polarizability. If one uses the Spitzer collision rate [79], the uniform density model tends to give an imaginary part of polarizability that is large only during brief times near resonance ($\varepsilon_{cluster} + 2 \approx 0$). The fluid simulations, on the other hand, indicate that the absorption occurs for a much larger time period due to the resonance at the critical surface. The modified collision frequency, Eq. (3.9), allows for this greater absorption. In particular, it provides a greater rate of collisions than the Spitzer formula, and the dependencies on density and temperature are chosen to match the hydrocode results for which the collective rate of absorption is largely independent of the collision frequency.

A comparison of the real and imaginary polarizability using the fluid model and our modified uniform density model is shown in Fig 3.1. In each case a 30nm cluster was irradiated with a laser pulse (100 fs FWHM, 800 nm wavelength) for three different peak intensities 5×10^{14} W/cm^2, 8×10^{14}W/cm^2, and 1×10^{15} W/cm^2. The basic time evolution of the polarizability is same for both the models. With regards to the optical property of the cluster, the validity of our model has been verified for the range of laser-cluster parameters considered in this work. Our simulations are valid for clusters of initial diameter of the order of a few hundred Angstroms, and laser

pulses of intensity 5×10^{14} W/cm^2 - 1×10^{16} W/cm^2 and pulse width of the order of 100 femtoseconds. These values are very typical of those measured or used in experiments. For parameters outside those considered here it is likely that modifications to the model would be necessary. The agreement between the two models starts failing as the density within the cluster falls below the critical density i.e. as the cluster disassembles. However, except for very long pulse-widths, this happens after the laser pulse has passed over the cluster and so is not important from the point of view of pulse propagation and self-guiding.

Clusters at different radial distances from the axis of propagation of the pulse will experience different temporal profiles of laser intensity due to the variation of intensity with radius. This will lead to a spatially and temporally varying effective dielectric constant through the variations of polarizability. Fig 3.2 shows a contour plot, in the r-ξ plane, of the real (a) and imaginary (b) polarizability for 30nm clusters irradiated by laser pulse (800nm, 100fs FWHM, 40μm radial FWHM, 1×10^{15} W/cm^2). After the clusters are ionized, the polarizability decreases with increasing radial distance in the region of rising Re(γ). Parts of the pulse that propagate through this region will be focused. After Re(γ) peaks and starts decreasing this trend reverses. The temporal variation in polarizability is also responsible for frequency shifts in the pulse spectrum. Specifically, rising Re(γ) will lead to red shifts in the spectrum while decreasing Re(γ) will cause the spectrum to blue shift. As seen in (b) the Im(γ) rises in magnitude only at a later time within the pulse. This should lead to a preferential strong absorption of the pulse tail. These effects are discussed in details when we present the results of numerical simulations of pulse propagation.

3.3 Laser Pulse Evolution

In this section we review the derivation of the laser envelope equations and discuss how these equations are combined with the cluster evolution equations of the previous section. We assume that the cluster gas is tenuous, having a small effective dielectric constant. In this case the laser pulse will evolve slowly as it propagates at nearly the speed of light. The laser field is then represented by a complex amplitude $\mathbf{E}_{\mathrm{L}}(\mathbf{x}_{\perp}, z, t) = \mathrm{Re}\{\hat{\mathbf{E}}_{\mathrm{L}}(\mathbf{x}_{\perp}, \xi, z)e^{-i\omega\xi}\}$ where ξ=*t*-*z*/*c* is a time variable in the laser frame. The effective dielectric constant is given by

$$\varepsilon = 1 + \delta\varepsilon(\mathbf{x}_{\perp}, \xi, z) = 1 + 4\pi n_c \gamma\,, \tag{3.10}$$

where n_c is the density of clusters, and $\gamma(\mathbf{x}_{\perp}, \xi, z)$ is the local average polarizability of clusters at the point ($\mathbf{x}_{\perp}$, z) and depends on time through the variable ξ. By average, we imagine that there are many clusters in a small volume whose size is small compared to the distance over which the laser envelope varies. In doing so we neglect Rayleigh scattering due to discreteness of the clusters. Finally, while cluster gases typically contain a distribution of cluster sizes, we will assume for the present that the average polarizability can be computed based on a single initial cluster size.

Applying the slowly varying envelope approximation, we can express the evolution of the envelope in terms of the variables $\mathbf{x}_{\perp}$, z, $\xi = t - z/c$, as

$$\left(\nabla_{\perp}^{2} + k_0^2 \delta\varepsilon_{eff} + 2ik_0 \frac{\partial}{\partial z}\right)\hat{\mathbf{E}}_{\mathrm{L}} = 0\,, \tag{3.11}$$

where $k_0 = \omega/c$. It is important to note that while Eq.(3.11) contains only a z derivative, the amplitude $\hat{\mathbf{E}}_{\mathrm{L}}$ and the effective dielectric constant $\delta\varepsilon_{eff}$ both depend on

time (ξ) in addition to z. The time variation of $\delta\varepsilon_{eff}$ is obtained by integrating the cluster expansion equations with t replaced by ξ.

Considering that clusters at different transverse locations experience different laser intensities the combined system of equations is complicated. As a first step, we will solve Eq. (3.11) using the Source-Dependent Expansion technique, following Esarey *et. al.* [80], in which the field envelope is expressed in terms of a series of Laguerre- Gaussian functions as

$$\hat{\mathbf{E}}_{\mathrm{L}} = \sum_{m=0,1,2,\ldots} \hat{\mathbf{E}}_m L_m(X) e^{-(1-i\alpha)X/2}, \tag{3.12}$$

where $\hat{\mathbf{E}}_m(\xi, z)$ is the complex amplitude, $L_m(X)$ is the Laguerre polynomial, $X = 2r^2/R^2$, $R(\xi,z)$ is the spot size, and $\alpha(\xi,z)$ is related to the curvature of the wave fronts. The expression for the field envelope is then substituted in equation (3.11) and truncated at the lowest order Gaussian mode assuming that the higher order modes are small and can be neglected. Extending the equations derived by Esarey *et. al.* [80] for the lowest order mode to the case of a complex dielectric constant, and putting $\hat{\mathbf{E}}_0 = \mathbf{E}_s e^{i\theta}$ we obtain the following equations to describe the parameters in (3.12):

$$\frac{\partial E_s}{\partial z} = -E_s\left(\frac{2}{k_0}\frac{\alpha}{R^2} + H_i + G_i\right), \tag{3.13}$$

$$\frac{\partial \theta}{\partial z} = -\frac{2}{k_0}\frac{1}{R^2} + H_r + G_r, \tag{3.14}$$

$$\frac{\partial R}{\partial z} = \frac{2}{k_0}\frac{\alpha}{R} + RH_i, \tag{3.15}$$

and,

$$\frac{\partial \alpha}{\partial z} = \frac{2}{k_0}\frac{1+\alpha^2}{R^2} - 2\left(H_r - \alpha H_i\right), \tag{3.16}$$

where

$$G_{r,i} = \frac{k_0}{2}\int_0^\infty dX\left(\delta\varepsilon_{r,i}e^{-X}\right), \tag{3.17}$$

and,

$$H_{r,i} = \frac{k_0}{2}\int_0^\infty dX\left(\delta\varepsilon_{r,i}(1-X)e^{-X}\right). \tag{3.18}$$

Here $\delta\varepsilon_r$ and $\delta\varepsilon_i$ are the real and imaginary parts of $\delta\varepsilon_{eff}$, the change in dielectric constant determined by the cluster response. Equation (3.13) describes the evolution of the field amplitude. The first term on the right describes the effect of diffraction while the second and third describes the effect of absorption. Equation (3.14) describes the evolution of the laser phase, $\theta(\xi, z)$. The ξ dependence of the phase gives the frequency shift on axis. Here time variations of the polarizability will contribute to the H_r and G_r terms and give frequency shifts. Equations (3.15) and (3.16) describe the evolution of the spot-size $R(\xi, z)$ and the phase front curvature $\alpha(\xi,z)$, with the first term in each equation describing the effect of diffraction. In addition to the diffractive terms, the radial dependence of the $\delta\varepsilon_{eff}$ will contribute to focusing and defocusing of the laser pulse. If $\delta\varepsilon_r$ and $\delta\varepsilon_i$ are peaked on axis then both H_r and H_i will be positive. The usual focusing effect due to an on-axis peak on $\delta\varepsilon_r$ is manifested by the H_r term in Eq. (3.16). A positive value of H_r causes the phase front curvature to become negative and leads to focusing through Eq. (3.15). There are additional defocusing effects associated with H_i. A positive H_i will cause defocusing in Eq. (3.15) due to preferential absorption of energy at small r and also leads to an increase in the curvature of the wave front.

We emphasize that the parameters E_s, θ, R, and α are functions of both axial distance z and laser frame time coordinate $\xi = t\text{-}z/c$. Equations (3.13) - (3.16) govern the evolution of these parameters in z with ξ being present as a parameter. The evolution of the laser pulse at different ξ values is coupled through equations determining the time dependent dielectric constant $\delta\varepsilon_{eff}(r,\xi,z)$. Basically, these are Eqs. (3.6)-(3.8) with the time derivative replaced according to $\partial/\partial t \rightarrow \partial/\partial\xi$. The heating rate in Eq. (3.8) depends on the intensity of the laser pulse, which has a Gaussian radial profile with a time and space varying amplitude and spot size. Solutions of this coupled system of equations will be explored in the subsequent sections.

3.4 Equilibrium and Stability of the Self-guided Solution

The focusing properties of the cluster plasma are described by the time dependent functions H_r and H_i defined by Eq. (3.18). These functions are proportional to the cluster density n_c and the time dependent polarizability γ. The polarizability depends on the properties of the laser pulse through the heating rate in Eq. (3.8).

We first consider the behavior of H_r and H_i when the laser pulse is specified to have a given energy, duration and spot size. Specifically we consider the case of a 100fs FWHM Gaussian envelope pulse centered at ξ=0 as in Fig 3.1(a). The time dependence of the polarizability leads to time dependent values of H_r and H_i. Accordingly, through Eq. (3.13)-(3.16) the pulse parameters E_s, θ, R, α will evolve in a time dependent way. Solutions of this process will be presented in the next section. Here we consider the values of H_r and H_i that are obtained at $\xi = 0$ fs corresponding to the peak of the injected pulse. The dependence of these quantities on spot size and

laser power will give insight into the guiding mechanism that occurs in cluster plasma. The values of the functions H_r and H_i are determined by first assuming that the radiation field has the following form, consistent with Eq. (3.12) truncated at one term,

$$\mathbf{E}_{\mathrm{L}}(\xi, r, z) = \mathbf{E}_{\mathbf{s}}(\xi, z) e^{i\theta(\xi,z) - (1 - i\alpha(\xi,z)) r^2 / R^2(\xi,z)}, \tag{3.19}$$

where for the moment we assume α and R are constants. We then solve Eq. (3.6)-(3.8) on a grid in r and compute the r and ξ dependent complex polarizability γ from Eq. (3.4). A sample of this is shown in Fig 3.2. The perturbed complex dielectric constant $\delta\varepsilon = 4\pi n_c \gamma$ is inserted in Eqs. (3.17) and (3.18), which are then numerically integrated in r to obtain $H_{r,i}$ and $G_{r,i}$.

We now consider the focusing of the pulse, which is determined primarily by H_r and H_i through Eqs. (3.15) and (3.16). Fig 3.3 shows plots of H_r and H_i at $\xi = 0$ fs versus the spot size R for a pulse of fixed energy (1.92mJ) and assuming $n_c = 3\times10^{11}$ cm^{-3}. The dependence of these curves on radius will determine the equilibrium and stability of guided states.

We first look for the equilibria by demanding $\partial R/\partial z = 0$ and $\partial\alpha/\partial z = 0$ in Eqs. (3.15)and (3.16). According to Eq. (3.15), in equilibrium $\alpha = -k_0 R^2 H_i/2$, that is, the phase fronts are slightly curved inwards. However, for the values of H_i indicated in Fig 3.3 and for the value $k_0 = 2\pi/\lambda = 7.85\times10^4$ cm^{-1} we find that $\alpha \ll 1$. Thus we further simplify our analysis by neglecting H_i and taking the equilibrium to be $\alpha = 0$, and $R = R_0$ where from Eq. (3.16)$H_r(R_0) = 1/k_0 R^2$. The quantity $(1/k_0 R^2)$ is also plotted on Fig 3.3 and we note that there are two possible equilibrium values where the H_r and

($1/k_0R^2$) curves intersect, (R = 28μm and R = 130μm). We will show later that only one of these values is stable.

An alternate way of specifying the equilibrium conditions is to note that H_r is proportional to the cluster density n_c. Thus, for any spot size R, we can adjust n_c until the equilibrium conditions are satisfied. This is shown in Fig 3.4 where the cluster density that will maintain the spot size at a fixed value is plotted for several values of pulse energy. It can be seen that for a given pulse energy there is a minimum cluster density required to have self-guided equilibria. In particular, for the case of pulse with energy 1.93 mJ (corresponding to a peak intensity of 1×10^{15} W/cm^2 for the pulse parameters of Table 3.1), this minimum cluster density is 4.2×10^{10} cm^{-3}. Also, for a given density there may be two or three equilibrium spot sizes.

We now study the stability of small perturbations away from the equilibrium for our simplified system. We consider the phase front curvature and spot size to be given by $\alpha = \delta\alpha(z)$ and $R = R_0+\delta R(z)$ where R_0 is the equilibrium spot size. Linearizing Eqs. (3.15) and (3.16) yields

$$\begin{aligned}\frac{\partial(\delta R)}{\partial z} &= \frac{2}{k_0}\frac{\delta\alpha}{R_0}\\ \frac{\partial(\delta\alpha)}{\partial z} &= -\left(\frac{4}{k_0 R_0{}^3}+2\frac{\partial H_r}{\partial R}\bigg|_{R=R_0}\right)\delta R\end{aligned}. \tag{3.21}$$

Note, we have again neglected H_i assuming $\alpha\ll1$. We look for exponential solutions of the form $\delta\alpha$ and $\delta R \sim \exp(\kappa z)$, and find

$$\kappa^2 = -\frac{4}{k_0 R_0{}^4}\left[2+\left(\frac{R}{H_r}\frac{\partial H_r}{\partial R}\right)\bigg|_{R=R_0}\right]. \tag{3.22}$$

Thus, the requirement for stability of an equilibrium is

$$\left(2H_r + R\frac{\partial H_r}{\partial R}\right)\Bigg|_{R=R_0} > 0, \tag{3.23}$$

where we note that H_r>0 is required for equilibrium. Note also that this condition does not depend on the cluster density, only the spot size, pulse energy and pulse duration matter.

The left-hand side of Eq. (3.23) is plotted vs. R_0 for several pulse energies in Fig 3.5. We see that in the 1.93 mJ case equilibria are unstable for 10μm<R<14μm and R>82μm. Thus, the 130μm equilibrium spot size found in the $n_c = 3\times10^{11}$ cm^{-3} case is unstable, while the R_0 = 28μm case is stable according to the simple model.

3.5 Numerical Simulation Results

In this section we present the numerical simulation results for the propagation of laser pulses through a clustered gas based on the coupled Eqs. (3.6)-(3.7) and (3.13)-(3.18). For the following numerical simulation results, the initial parameter values for the cluster and the laser field are given in Table 3.1 These parameters are similar to those typically seen in the laboratory. Unless otherwise mentioned the results refer to quantities at ξ=0, the center of the laser pulse.

Table 3.1 Initial Conditions for numerical simulation of laser pulse propagation through clustered gas

Pulse	Cluster
Wavelength = 800nm	Initial radius = 30nm
Pulse width = 100fs FWHM	Threshold intensity for ionization = 1×10^{14} W/cm^2
Peak Intensity = 1×10^{15} W/cm^2	Degree of ionization = 9
Spot size = 40μm FWHM	Ion density = 1.8×10^{22} cm^{-3} = $10n_{critical}$
Phase(θ) = 0	Cluster density = 2.19×10^{11} cm^{-2}
Curvature(α) = -.1284 (determined by equilibrium conditions at ξ=0)	(determined by equilibrium conditions at ξ=0)
Energy = 1.93 mJ	

Contrary to the low energy absorption when a tenuous gas is irradiated by laser, clustered gases absorb laser energy very efficiently. This has an important impact on the applications of the laser-cluster interaction process like x-ray production and generation of energetic particles. Fig 3.6 shows the power within the pulse for different distances of propagation. The laser-cluster system was initialized to the values in Table 3.1. As seen in the figure, the power is quickly absorbed at the tail end of the pulse, while the front remains un-attenuated. Absorption of pulse energy is due to the positive imaginary part of the complex cluster polarizability. The strong absorption of laser energy at latter times in the pulse is a consequence of the sharp rise in Im(γ) at those times (see Fig 2.1). The front of the pulse, where the

intensity is below the critical intensity for ionization of the cluster, propagates through unionized clusters and is not absorbed.

Fig 3.7 shows the evolution in energy and spot size of the pulse with propagation distance z, for the initial conditions in Table 3.1.We note that by 1.5 cm the pulse has deposited 83% of its energy in the gas. After this the pulse energy changes little. Two measures of the spot size are plotted: the instantaneous spot size at $\xi = 0$ and the RMS spot size weighted by the time-dependent pulse power. The spot size for propagation through vacuum is plotted for comparison and to illustrate the guiding effect. Both the instantaneous and RMS spot sizes expand less in clustered gas medium than in vacuum. The effective Rayleigh length in this case is seen to be ~1.2 cm while that in vacuum is 0.45 cm. The center of the pulse however, as seen via $R(\xi=0\text{fs},z)$ remains distinctly focused for more than 1.5 cm. Such self-focusing has been experimentally observed by Alexeev *et al.* [17] where they focus a 7.5 mJ, 800nm pulses with pulse widths in the range 80fs-1.4ps into clustered argon gas.

Next we try to explore the effect of initial energy on the focusing property of the interaction for a fixed pulse width. A comparison of the laser beam RMS spot size is plotted in Fig 3.8 for the different initial energies. For this simulation, pulses of different initial energy (set by varying the peak initial intensity) were propagated through clustered gas having the initial laser-cluster parameters as in Table 3.1 but the cluster density was set to 3×10^{11} cm^{-3} and the initial curvature α was set to zero. It is seen, for such a configuration, that we achieve optimal guiding for intensities around 2×10^{15} W/cm^2. For lower energies, the pulse intensity falls below the threshold value very soon causing the pulse to diffract in the medium of unionized clusters. For

higher peak intensities, a larger temporal portion of the pulse faces a defocusing profile of Re(γ), as seen in Fig 3.1, causing the RMS spot size to be larger.

A comparison of the energy absorbed versus propagation distance is plotted for each of these cases in Fig 3.9. We note that the rate of absorption of laser energy increases as we increase the initial energy. Higher peak intensity results in a larger value of the imaginary part of polarizability γ leading to a higher value of H_i and G_i. These directly lead to an increased attenuation rate for the laser field amplitude (and thus energy) via Eq. (3.13). Moreover, greater peak intensity causes clusters to ionize and thus absorb laser energy over a larger radial zone. As the pulse advances, however, a reduced intensity laser field has lesser potential for ionization and further absorption. Thus the rate of energy absorption tapers off.

As the pulse propagates, different parts of the pulse experience different dielectric constants, due to the time-dependence of the cluster polarizability γ. Thus the pulse picks up a time-dependent phase leading to local frequency shift or chirp, $\Delta\omega$. This is given by

$$\Delta\omega = -\frac{\partial\theta}{\partial t} \tag{3.26}$$

and represents the frequency shifts on axis (r =0). Fig 3.10(a) and (b), respectively, show the variation in the on axis phase and the chirp within the pulse, at different distances of propagation. Around ξ=-80fs, the phase shows a sudden rise, leading to a red shift as seen in the chirp. At this time, the intensity of the pulse exceeds the threshold intensity causing ionization and a positive jump in the polarizability that appears as a frequency red shift. At z = 0.72 cm there is a sudden kink in phase for ξ = 86fs. This is reflected in the chirp as a strong red shift. The position of this kink

moves towards increasing ξ with z. Also, as seen in Fig 3.10(c) the spot size R shows a sharp focusing at the same position where the kink occurs in phase. This time dependent focusing in the pulse gives rise to the kink in phase and the associated red shift.

To understand this focusing we examine the governing equations more closely. From Eq. (3.14) we see that the evolution of the phase is governed by three terms - the first term, which is the diffraction term, and contributions due to the real polarizability, the H_r, and G_r terms. Since all the three terms are functions of spot size R, the variation in R is significant in understanding the behavior of the phase. Fig 3.11 shows the evolution of the (a) spot size (R), (b) curvature (α), and (c) phase (θ) for two different ξ values (ξ=86 fs and ξ=101 fs) around the region where the kink occurs in phase. The curve corresponding to ξ=0 fs is provided for comparison. The initial pulse parameters were selected so that the ξ =0 fs portion of the pulse is in equilibrium and as seen in Fig 3.11 the spot size and curvature at ξ = 0 remain relatively constant. Other parts of the pulse do not start in an equilibrium state and the spot size and curvature vary with distance. Let us consider these non-equilibrium curves. Initially both H_r and H_i are positive while the phase front curvature α is close to zero. Consequently, the spot size R will increase according to Eq. (3.15) and α decreases because the focusing term $2H_r$ in Eq. (3.16) is larger than the diffractive term, $2/(k_0R^2)$. As the phase front curvature becomes more negative the rate of increase in spot size decreases and eventually the spot size begins to decrease. That is, the pulse begins to focus. As the spot size decreases, the diffraction term in Eq. (3.16) becomes more important and the phase front curvature α begins to increase. At the

focal point, where the spot size attains its minimum value the curvature is approximately zero. After the focal point the curvature and spot size increase as in simple diffraction. As the spot size R passes through its minimum value at the focal point there is an abrupt decrease in phase due to the first term in Eq. (3.14). This decease in phase occurs earlier for the portion of the pulse at $\xi = 86$ fs than for the portion of the pulse at $\xi = 1001$ fs, as is shown in Fig 3.11c. Consequently, the phase as a function of ξ at fixed z shows a sharp increase at the ξ location separating portions of the pulse that have already focused from those which are yet to focus.

The on-axis frequency shift $\Delta\omega = \partial\theta/\partial\xi$ describes the change in the frequency components at $r = 0$. In the previous example we have seen that the phase aquires a time dependence because of the moving focus and the diffractive term, $-2/(k_0R^2)$ in Eq. (3.14). The abrupt change in phase that occurs as a portion of the pulse passes through a minimum in spotsize is a linear effect. The same term is responsible for the Guoy phase shift that occurs when a Gaussian beam is focussed. The pulse's frequency components are actually changed due to the time dependence of the phase, the spot size, and the phase front curvature that occurs due to the time dependent medium. These different spectral components then arrive at the axis at different times giving rise to the abrupt change in the on-axis phase. A quantity which is indicative of the radially averaged frequency is

$$\Delta\varpi(\xi, z) = -\operatorname{Im}\left\{\int_0^\infty 2\pi r dr \mathbf{E}^* \partial\mathbf{E}/\partial\xi\right\} / \int_0^\infty \left(2\pi r dr \left|\mathbf{E}\right|^2\right). \tag{3.27}$$

Using Eq. (3.19) we find this to be given by

$$\Delta\varpi = -\left(\frac{\partial\theta}{\partial\xi} + \frac{R^2}{2}\frac{\partial}{\partial\xi}\left(\frac{\alpha}{R^2}\right)\right). \tag{3.28}$$

According to Eq. (3.14)-(3.16) this quantity satisfies

$$\frac{\partial}{\partial z}\Delta\varpi(\xi, z) = -\left(\frac{\partial G_r}{\partial\xi} + \frac{2H_r}{R}\frac{\partial R}{\partial\xi}\right) - H_i R^2 \frac{\partial}{\partial\xi}\left(\frac{\alpha}{R^2}\right). \tag{3.29}$$

The first term on the right side of Eq. (3.29) describes the effect of the changing real part of the dielectric constant on the frequency. We note, from Eqs. (3.17) and (3.18) that

$$\left(\frac{\partial G_r}{\partial\xi} + \frac{2H_r}{R}\frac{\partial R}{\partial\xi}\right) = \frac{k_o}{2}\int_0^\infty dX\left(\frac{\partial\delta\varepsilon_r}{\partial\xi}\right)e^{-X}. \tag{3.30}$$

The second term on the right represents the effect of radial variations in the absorption on the radially averaged frequency shift. A plot of $\Delta\varpi(\xi,z)$ vs. ξ for different distances of propagation is shown in Fig 3.10(d) for a laser-cluster system initialized to conditions in Table 3.1. A red shift in frequency occurs at the time when the cluster ionizes. Also, the figure indicates a strong red shift at times when the kink occurs in phase. However, we should note that a high negative (positive) value of the radial averaged frequency shift will not translate to a strong red (blue) shift in the pulse spectrum if the power at that location is very small. Thus a better measure of the effect on the pulse spectrum would be given by the radial averaged frequency shift weighted by the power. This is plotted in Fig 3.10(e). It indicates strong red shift at time of ionization of clusters and due to the time-dependent dielectric constant. This should lead the pulse spectrum to be red shifted. For our pulse of 100fs FWHM, there is very little power at the location in the pulse where the kink occurs. Thus this abrupt change in phase does not have a strong effect on the pulse spectrum. However,

this effect may become important for pulses of longer duration. This is yet to be explored.

The pulse spectrum at different distances of propagation, $z = 0$ cm, 0.3 cm, 0.6 cm, 0.9 cm and 1.2 cm, is plotted in Fig 3.12. As the pulse propagates it spreads in frequency due to the temporal behavior of Re(γ). A rising Re(γ) causes a red shift while decreasing Re(γ) causes the pulse spectrum to have a blue shift. Additional red shift occurs due to the development of the moving focus described above. Such spectral broadening is also consistent with recently reported experimental results [37].

3.6 Summary and Conclusions

We have described a self-consistent model for the simulation of laser pulse propagation through a gas of exploding clusters. Stability and equilibrium of the system are also studied. We find that for typical laser cluster parameters there are multiple equilibria but not all of them will be stable. For our particular case, we found two sets of parameters that support equilibria but only one was found to be stable. Also, there is a minimum required cluster density for equilibrium of a pulse with fixed energy. For example, in our case of 1.93mJ pulse, this minimum cluster density was 4.2×10^{10} cm^{-3}.

Our simulations indicate that starting from an equilibrium value the laser pulse typically remains focused for distances of the order of 1.5 cm. The focusing length, however, varies with the pulse peak intensity (other parameters remaining constant), and for the system considered we obtained the maximum focusing distance for a pulse of peak intensity 2×10^{15} W/cm^2. There is very efficient coupling of the laser energy to the clusters, far exceeding that in case of interaction of a laser pulse

with a low-density un-clustered gas. By the time the laser propagates 1.5 cm through the clustered gas more than 80% of its energy is absorbed. The simulations suggest rapid absorption of energy by the clusters during the initial part of the propagation and the rate of absorption falls off with propagation distance. Also, a pulse with higher initial energy was absorbed much faster than a pulse with lower energy. This efficient absorption of laser energy by the clusters is an important property with respect to the applications. The pulse is frequency shifted as it propagates. This is primarily due to the temporal variation in the cluster complex polarizability leading to a time-varying dielectric constant. Also as the pulse propagates, it develops a moving focus reflected as a kink in the on-axis phase. This, along with the time dependence of polarizability, leads to a red shift in the pulse spectrum.

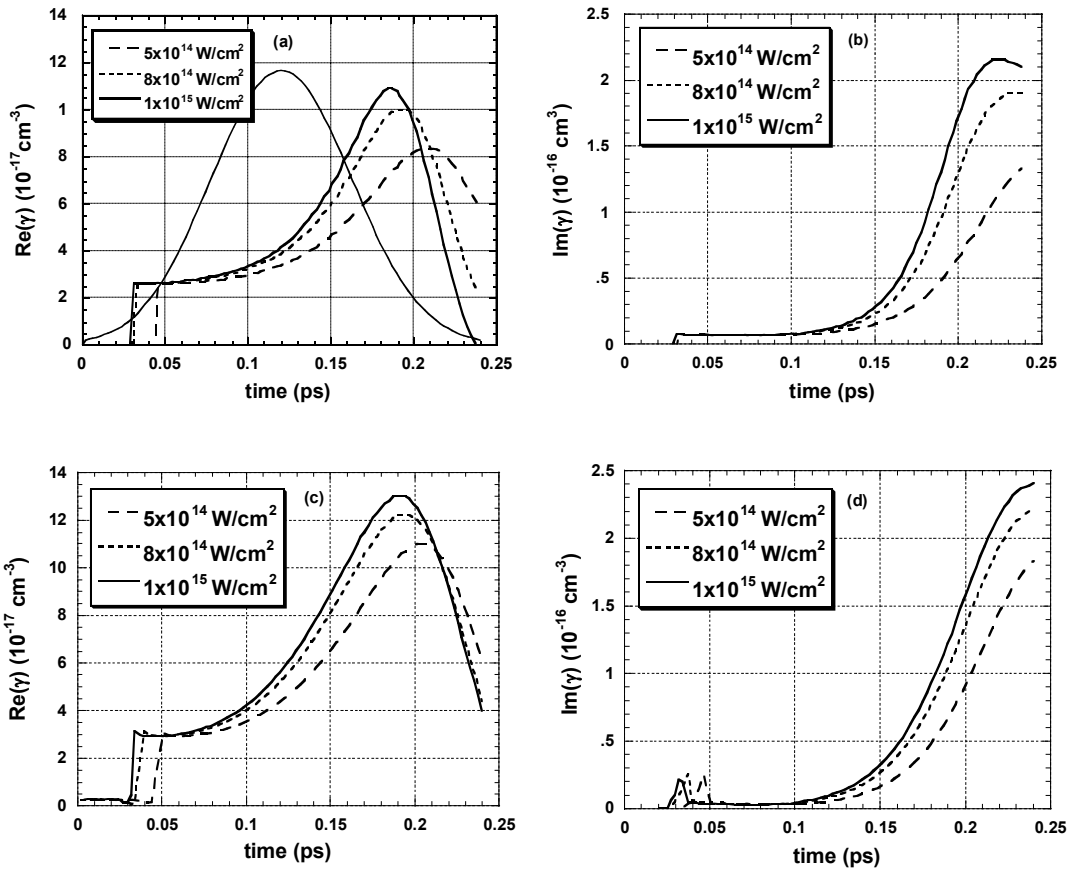

Fig 3.1 A comparison of the real and imaginary polarizability for our model (a,b) and the hydrocode of Milchberg (c,d). In each case, a cluster of initial radius 30nm is irradiated with a 800nm, 100 fs FWHM laser pulse for three different peak intensities 5×10^{14} W/cm^2 (dashed), 8×10^{14}W/cm^2 (dotted), and 1×10^{15} W/cm^2 (solid -dark). The pulse profile is shown in (a) as a thin solid line.

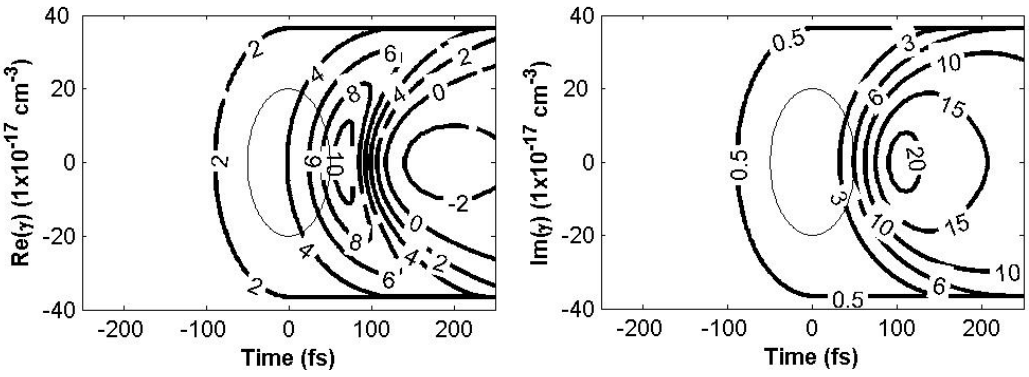

Fig 3.2 Contour plot of (a) real and (b) imaginary part of polarizability in the r-ξ plane. The ellipse in the center of each plot marks FWHM points.

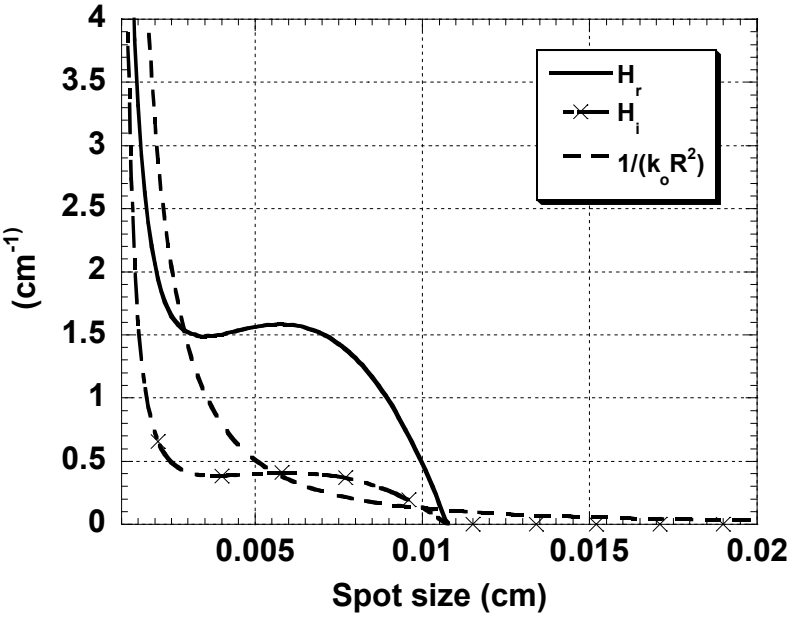

Fig 3.3 The quantities $H_r(\xi=0$ fs) (solid) and $H_i(\xi=0$ fs) (dashed with cross markers) are plotted at z = 0.006 cm. Here, the cluster density set to $n_c = 3\times10^{11}$ cm^{-3} and the spot size of the pulse was varied from 10μm to 200μm. All other parameters were initialized to the conditions in Table 3.1. The intersection of H_r with the $1/k_0R_0^2$ curve (dashed) gives the equilibrium values of R for the chosen cluster density.

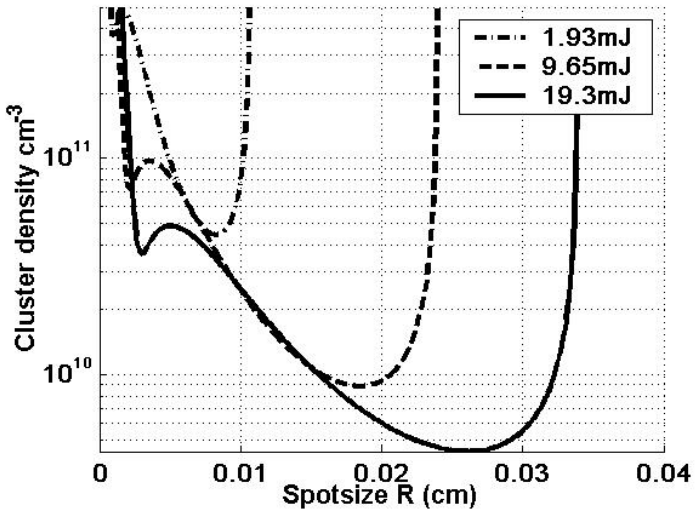

Fig 3.4 Cluster density required for equilibrium of a pulse as a function of the pulse spot size for three different initial energies 1.93 mJ (dash-sot), 9.65 mJ (dashed), and 19.3 mJ (solid). All other parameters were initialized to the conditions in Table 3.1. Note that for a pulse with given initial energy the same cluster density can occur for two values of *R*

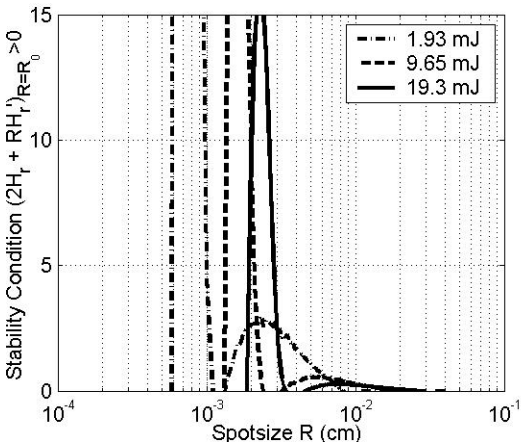

Fig 3.5 Stability expression $(2H_r + R\partial H_r/\partial R)_{R=R0}$ vs. spot size R for a laser beam for three different initial pulse energies 1.93 mJ (dash-dot), 9.65 mJ (dashed), and 19.3 mJ (solid) All other parameters initialized to the conditions in Table 3.1. The range of R over which the plotted quantity is positive is stable. For example, in the 1.93mJ case, the region of stability corresponds to 14μm<R<82μm and R<8μm

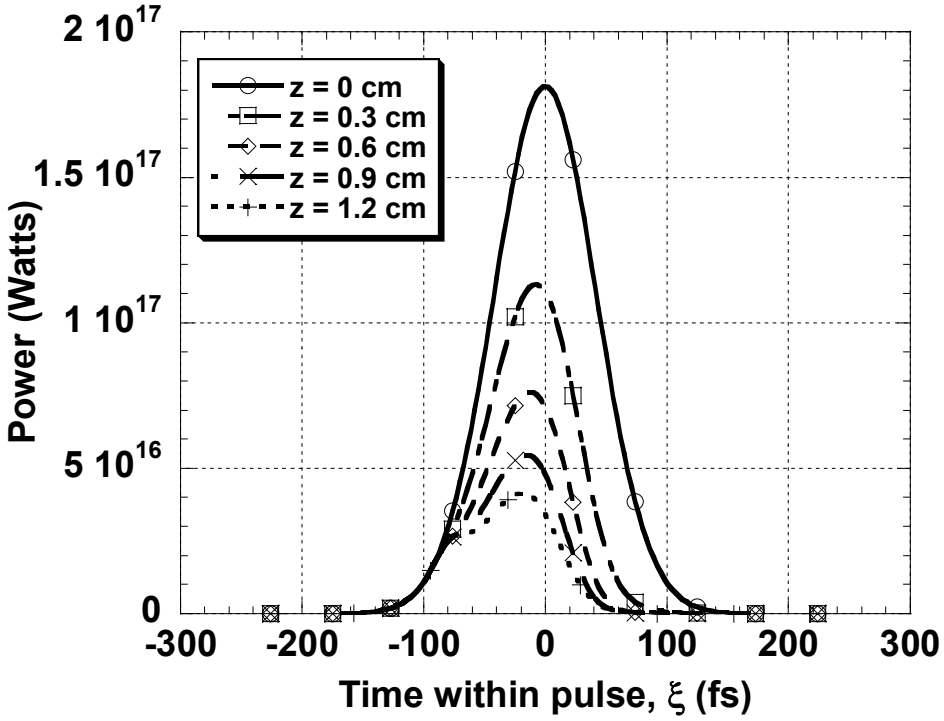

Fig 3.6 Power within the pulse (initial parameters of Table 3.1) at z = 0cm, 0.3 cm, 0.6cm, 0.9 cm and 1.2 cm. The front of the pulse, traveling through unionized clusters, does not get absorbed and hence propagates unattenuated while the trail end (where the imaginary part of polarizability is high) is strongly attenuated.

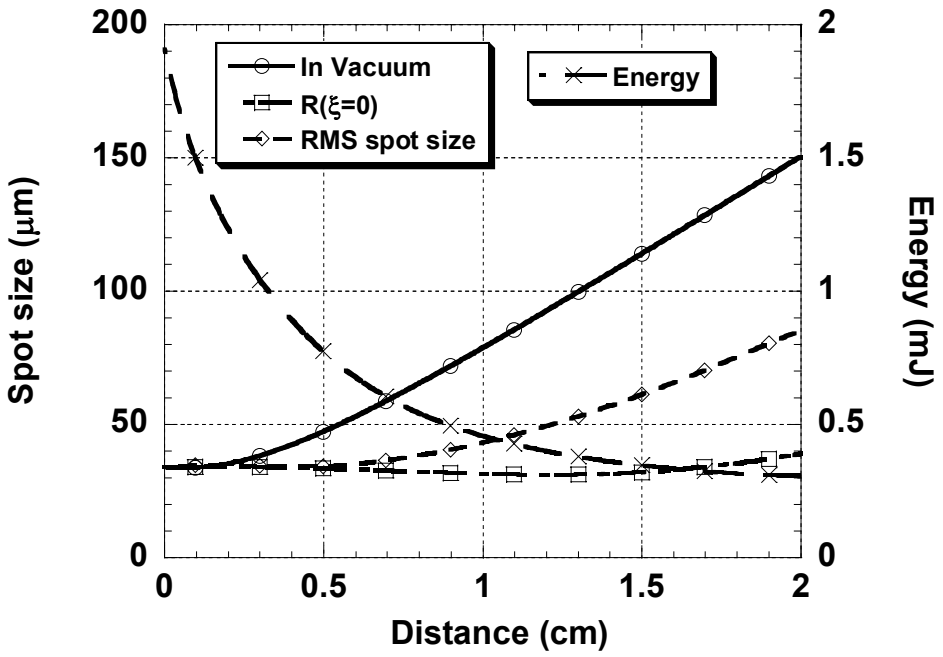

Fig 3.7 Self-guiding of the laser pulse in cluster medium. The figure shows the spot size at the center of the pulse ($\xi = 0$ fs) (dashed with square marker) for propagation through 2.0 cm of clustered gas for the initial conditions of Table 3.1. The result for propagation through vacuum (solid with circle markers) is plotted for comparison. The RMS (root mean squared) spot size is also shown (dashed with diamond markers). The center of the pulse remains focused for roughly 1.5cm. The energy within the pulse (solid with cross markers) is plotted in mJ (right axis). We note that about 83% of the pulse energy is absorbed by the clusters in 1.5 cm of propagation, after which the rate of absorption levels off.

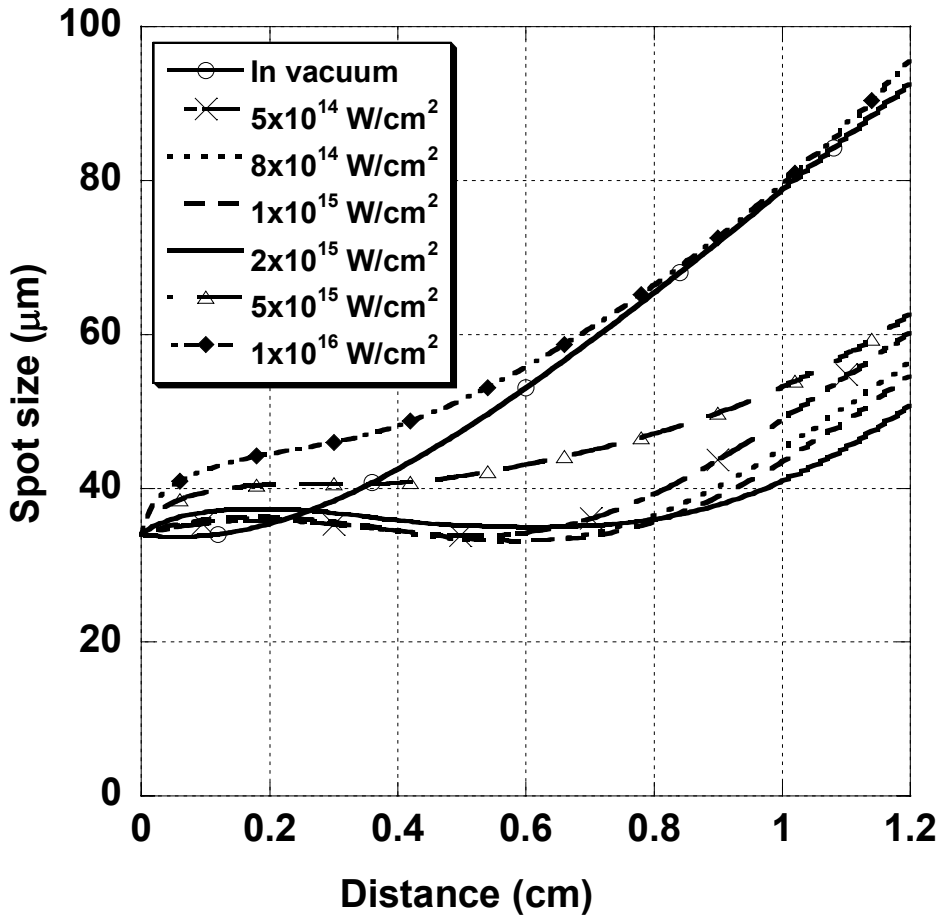

Fig 3.8 RMS spot sizes as a function of propagation distance for pulses with six different initial peak intensities: 5×10^{14} W/cm^2, 8×10^{14}W/cm^2, 1×10^{15} W/cm^2, 2×10^{15} W/cm^2, 5×10^{15} W/cm^2, and 1×10^{16} W/cm^2. Here cluster density was set to $n_c = 3\times10^{11}$ cm^{-3}, other initial conditions being those in Table 3.1. We note that the guiding effect is strongest around peak intensity of 2×10^{15} W/cm^2. The evolution of spot size for a pulse propagating in vacuum is plotted for comparison.

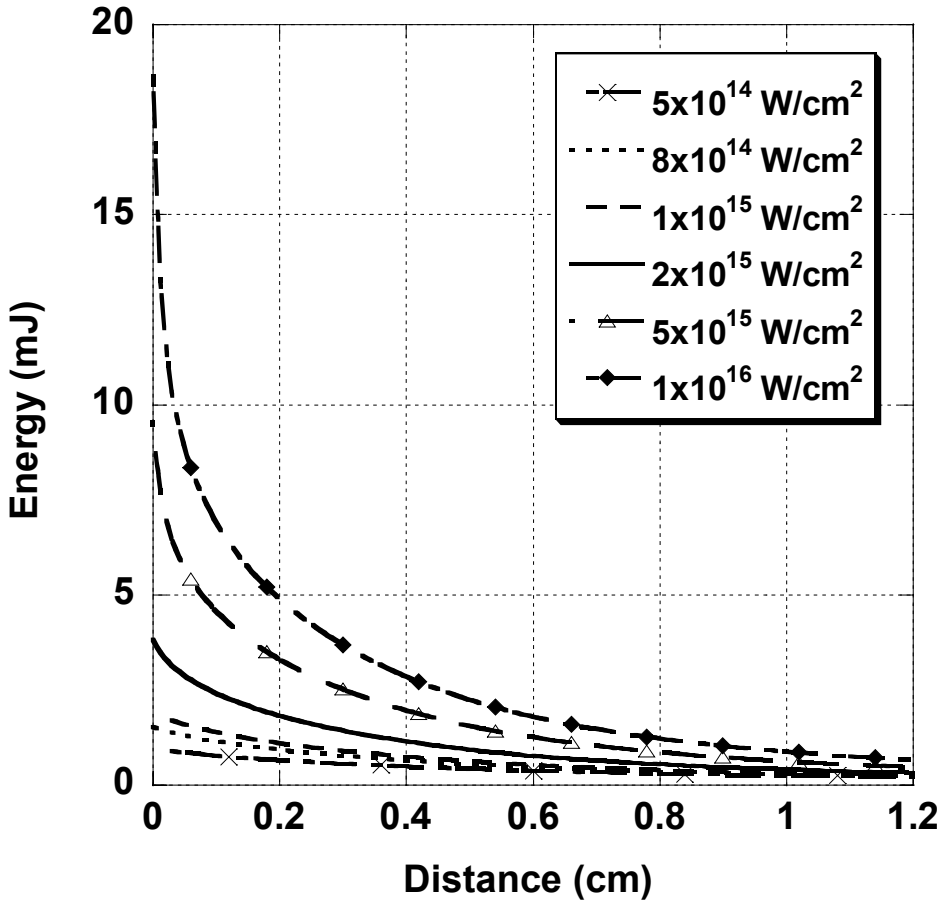

Fig 3.9 Variation of energy within the pulse with propagation for pulses of different initial peak intensities: 5×10^{14} W/cm^2, 8×10^{14}W/cm^2, 1×10^{15} W/cm^2, 2×10^{15} W/cm^2, 5×10^{15} W/cm^2, and 1×10^{16} W/cm^2. Here cluster density was set to $n_c = 3\times10^{11}$ cm^{-3}, other initial conditions being those in Table 3.1. Pulses with higher initial energy have a higher rate of energy absorption initially. As the pulse energy gets depleted the rate of absorption falls.

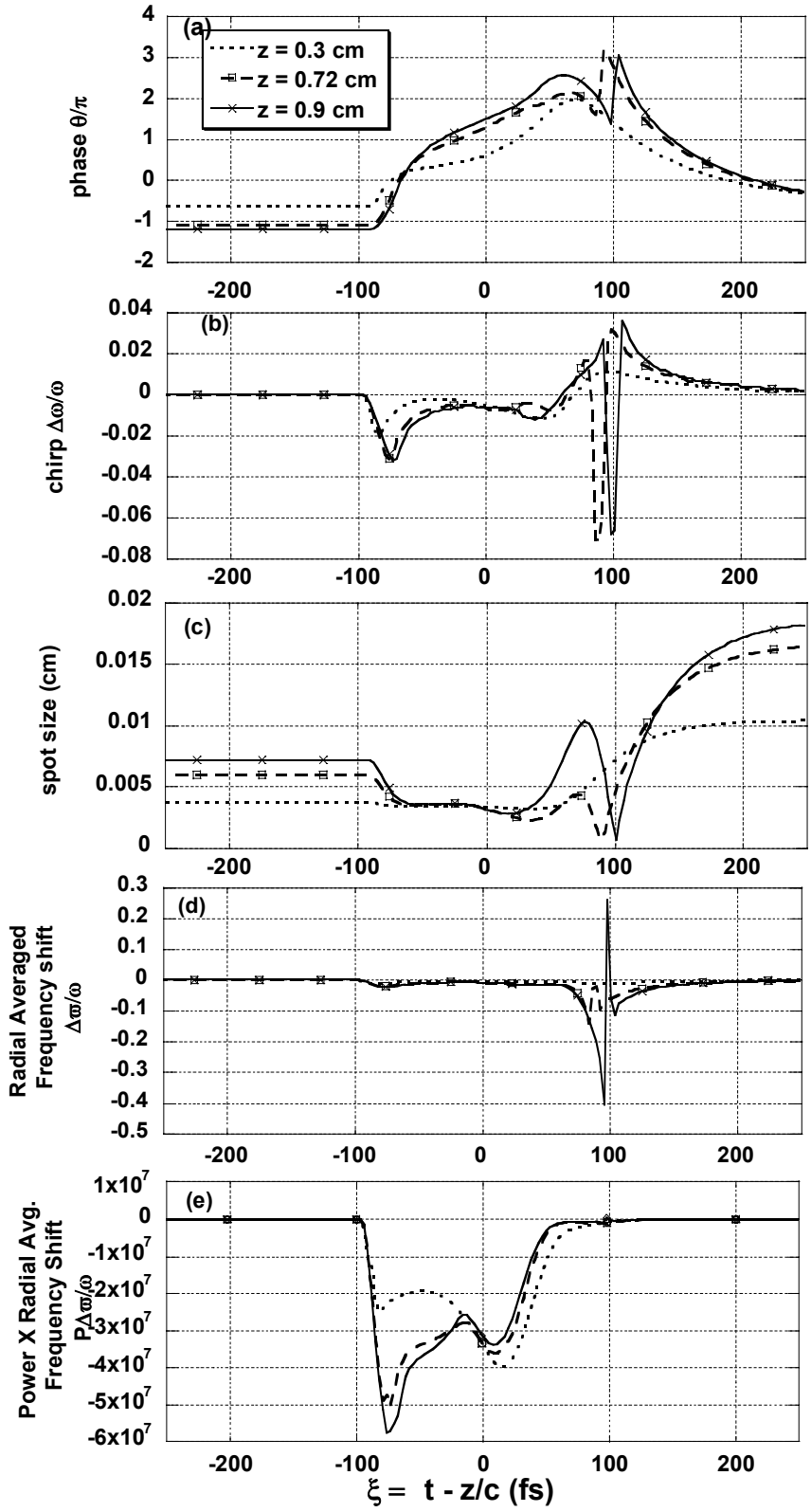

(see caption on next page)

Fig 3.10 (a) Phase, (b) chirp developed, (c) spot size of the pulse, (d) radially averaged frequency shift, and (e) power weighted radial averaged frequency shift, at z = 0.3 cm, 0.72 cm, and 0.9 cm (for initial conditions of Table 3.1). The rise in phase at ξ =-80 fs is due to ionization and appears in (b) and (d) as a red shift. The z = 0.72 cm curve shows a kink in phase at around ξ= 86 fs. This is due to the sharp focusing of the pulse as seen in (c) and provides further red shift as seen in (b) and (d). The frequency shift weighted with power gives the effect of the propagation on the pulse spectrum.

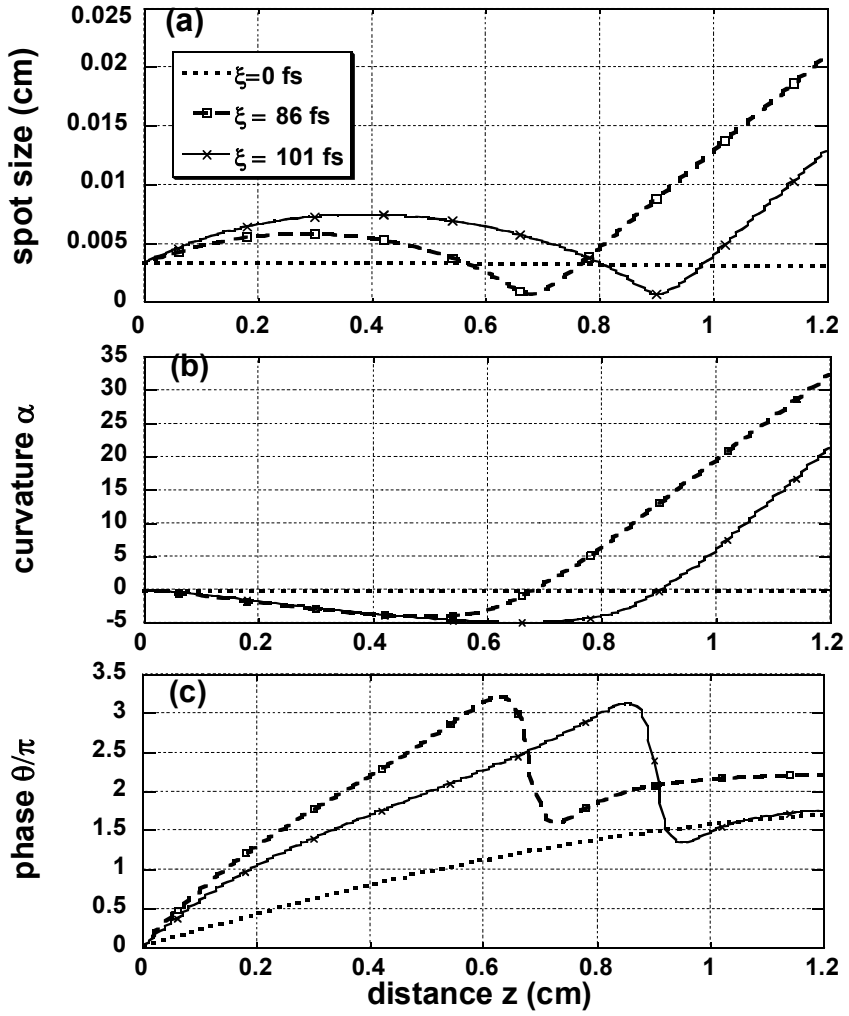

(see caption on next page)

Fig 3.11 Variation with propagation distance of spot size (a), curvature (b) and phase (c) of the pulse at three different locations within the pulse (ξ= 0 fs, 86 fs, 101 fs). The moving focus seen in (a) causes a sharp fall in phase (c).

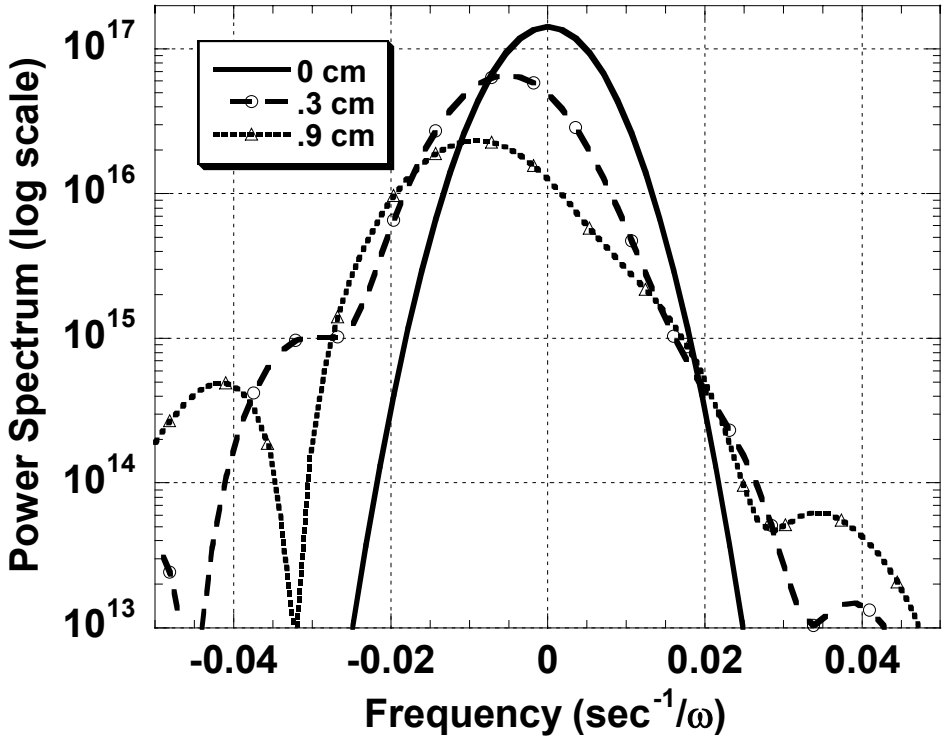

Fig 3.12 Power spectrum of the pulse (in logarithmic scale) for z = 0 cm, 0.3 cm and 0.9 cm. We see the spectrum broadening with propagation and significant red shifting of the initial spectrum.

4 Laser Pulse Spectrum Evolution and Effect of Hot Electrons on pulse propagation through clustered gases

4.1 Introduction

In the previous Chapter, we described the non-linear propagation of laser pulses through a gas of atomic clusters. The clustered gas was modeled as a non-linear optical medium with an evolving refractive index dependent on the transient complex polarizability of an individual cluster. An effect that depends on the same transient behavior of polarizability is the occurrence of frequency shifts as a result of the self phase modulation of the laser pulse as it propagates through the exploding cluster gas. In a clustered gas jet, Kim *et. al.* [37] have observed red shifts in the spectrum of the scattered and transmitted radiation at moderate intensities ~10^{15} W/cm^2. However, the observation of red shifts owing to the propagation of intense pulses in plasmas has been previously restricted to the case of ultra-intense pulses in the relativistic regime, where the refractive index change owing to relativistic mass increase leads to self-focusing red shifts [81, 82]. At moderate intensities in non-clustered gas jets, only blue shifts from ionization are observed [83, 84]. Measurements of intensity and spectrum of laser pulses scattered by and transmitted through a gas of atomic clusters [37, 64, 66, 85] provide some valuable diagnostic tools to understand the time-dependent explosion dynamics of laser-heated clusters. In this Chapter we extend our model to allow for a fraction of the gas to be present as unclustered atoms (monomers) and include the effect of monomer ionization on the medium refractive index. In the next section we discuss the results of our simulations

to explain the experimental results obtained by Kim *et. al.* [37]. The work presented in this Section was published in reference [37].

In the latter part of this Chapter we refine our laser-cluster interaction model to include the effect of energetic electrons. Particle-in-Cell simulations of laser-irradiated clusters indicate that even for laser pulses with moderate peak intensities (~ 10^{15} W/cm^2) the laser pulse extracts electrons from the cluster and accelerates them, creating a population of 'hot' electrons that are not bound by the cluster potential. These unbound energetic electrons are expected to contribute to the background electron density and modify the optical response of the cluster [53]. A limitation of the fluid model for cluster heating presented in Chapter 3 is that it does not take into account the effect of these hot electrons on the refractive index of the medium. Here we extend that model to incorporate the effect of the energetic electrons on the transient complex polarizability of a cluster. Simulation results for propagation of laser pulses through clustered gas, using this new model, are presented in Section 4.3 This work has been published in reference [86].

4.2 Spectral Shifts in Intense Laser-Clustered Gas Interaction

The setup used by Kim *et. al*. [37] is shown in Fig 4.1. Ti:Sapphire laser pulses (1.5 mJ, 798 nm), of variable width in the range of 80 fs – 1.5 ps, were focused into a gas of argon clusters in the range of peak intensities of 5x10^{13} – 10^{15} W/cm^2. The average radius of clusters was estimated to be ~300 Å at a backing pressure of 400 psi [42]. The full beam path through the argon jet (2 mm above the conical nozzle orifice) was ~3 mm. The beam at the exit of the jet was relay imaged to the entrance slit of an imaging spectrometer, which collected a one-dimensional (1D)

space-resolved spectrum of the exit beam mode. The mean transmitted wavelength, λ_{trans}, obtained from 50-shot averaging, is plotted in Fig 4.2 as a function of chirped pulse duration and sign. The positive or negative sign in the pulse duration indicates the pulse chirp direction. For a positive chirp, the instantaneous laser frequency changes from lower to higher frequency, or red to blue, with time, and vice versa for a negative chirp. Fig 4.2 shows that positively chirped pulses are largely red shifted after propagation through the gas of argon clusters and monomers, while negatively chirped pulses are blue shifted. However, the variation of λ_{trans} is asymmetric with respect to chirp sign, with some blue shifting occurring for short positively chirped pulses, and with the red shift for longer positively chirped pulses larger than the blue shift for similar negatively chirped pulses.

In an effort to understand the observed results, we consider laser pulse propagation through the clustered gas jet modeled as a combination of clusters and background neutral monomers. Both the clusters and the monomers are ionized by the laser pulse and contribute to the effective refractive index given by

$$n_r(t) = \left(1 + 4\pi N_c \bar{\gamma}_r(t) - N_e(t)/N_{cr}\right)^{1/2} \simeq 1 + \left[2\pi N_c \bar{\gamma}_r(t) - \tfrac{1}{2} N_e(t)/N_{cr}\right] \qquad (4.1).$$

where $\bar{\gamma}$ is the effective average polarizability for an ensemble of cluster sizes, N_c is the number density of clusters, $N_e(t)$ is the electron density deriving from ionization of the unclustered atoms (monomers), and $N_{cr} = m\omega^2/4\pi e^2$ is the critical density, where m and e are the electron mass and charge and ω is the laser frequency. Kim *et. al* have measured the evolution of the transient complex polarizability of clusters [73]. In general γ_r=Re(γ) initially increases in time as the cluster expands. The polarizability remains positive as long as the cluster response is dominated by plasma which is

above critical density. After sufficient cluster expansion, when the dominant response is by the sub critical plasma, γ_r becomes negative. At the same time, γ_i=Im(γ) is increasing and reaches its peak near the zero crossing of γ_r. In the frequency domain, this transient behavior of polarizability is seen as self-phase modulation and frequency shifts in the laser spectrum. The transient spectral shift can be expressed as

$$\delta\omega(t) = 2\pi L\lambda^{-1}\tfrac{d}{dt}n_r(t) = 2\pi L\lambda^{-1}\tfrac{d}{dt}\left[2\pi N_c\bar{\gamma}_r(t) - \tfrac{1}{2}N_e(t)/N_{cr}\right] \qquad (4.2)$$

where λ is the laser central wavelength, L is the propagation path length through the heated cluster plasma. The first term on the right hand side of Eq.(4.1) is the contribution of the exploding clusters to shifts in the pulse spectrum while the second term is the contribution due to the changing background electron density from ionization of monomers.

A possible explanation for the observed asymmetry at short pulse durations in Fig 4.2 is that a contribution to blue shifts originates from ionization of monomers in the gas flow [28]. Early in the laser pulse, optical field ionization (OFI) occurs for both monomers and for atoms in clusters. For a sufficiently short pulse, OFI of the monomers could occur before the cluster polarizability $\bar{\gamma}$ reaches its maximum value, which is achieved after some heated cluster expansion [4,5]. The ionization of monomers would induce a transient response of the refractive index and a blue shift in λ_{trans}, via the second term in Eq. (4.2). For longer pulse durations, the laser intensity decreases and the OFI of non-clustered monomers is greatly reduced compared to the efficient laser-driven collisional ionization of the clusters. This is consistent with the observation that the red shifts of longer positively chirped pulses are much stronger than the blue shifts for the corresponding negatively chirped pulses. Thus at long

pulse durations the cluster response would dominate and spectral red shifts are expected when $\bar{\gamma}_r$ increases with time as the clusters ionize and expand in the presence of the laser field. However, the evolution of $\bar{\gamma}_i$ can mask observation of the spectral changes induced by a transient $\bar{\gamma}_r$. Since $\bar{\gamma}_i$ increases later in the pulse [73], with positive chirped pulses, the later (blue) frequency components undergo more absorption and scattering out of the beam and this can shift $\bar{\lambda}_{\text{trans}}$ to the red. For negatively chirped pulses, the later red frequency components are preferentially absorbed and scattered, resulting in a blueshift in $\bar{\lambda}_{\text{trans}}$.

We also perform simulations of propagation of chirped laser pulses through the clustered gas using our self-consistent model presented in Chapter 3. The model makes the simplifying assumption of considering only the lowest order Gaussian mode of the laser pulse, with amplitude, phase, spot size and phase front curvature that vary slowly in space and time. The refractive index of the medium is modeled via Eq. (4.1). For ease of computation, the average polarizability of the cluster ensemble $\bar{\gamma}$ is substituted with the individual cluster polarizability from our modified uniform density model for the cluster. This enables us to use an experimentally consistent time-dependent complex polarizability of an individual cluster without sacrificing computational speed. The rate of ionization of monomers is governed by the optical field ionization or tunneling ionization equations of reference [87].

Fig 4.3 shows the simulated mean wavelength, λ_{trans}, of the transmitted pulse for a sequence of chirped incident pulses in the range of 80fs to 1.5 ps, with peak intensity in the range of 5×10^{13}-10^{15} W/cm^2. The incident pulse bandwidth, centered at $\lambda = 798$ nm, is commensurate with an 80 fs full width at half maximum (FWHM)

Gaussian pulse. As in the experiments, the vacuum beam waist was placed at the center of a 3-mm long medium. The initial size of a cluster was taken to be 300 Angstroms. The fraction of the total number of atoms present as clusters was varied from 25% to 75%, and the volume average gas density was adjusted such that the electron density at long times after cluster explosion (3.8×10^{18} cm^{-3}) was consistent with interferometric measurements.

For cluster fractions of between 25% and 50%, the simulation results reproduce the ~6 Å asymmetric blue shift for short pulses and the ~2 Å red shift for the longer (+) pulses, both seen in Fig 4.2. However, for longer (–) pulses, the simulation predicts a blue shift of ~3 Å, which is significantly larger than what is seen in Fig 4.2. This discrepancy is not understood at this present time, and maybe related to a small pulse-shape asymmetry in the experimental positive-chirped and negative-chirped pulses. Increasing the cluster fraction (reducing the monomer fraction) is seen to remove the asymmetric blue shift, and the result for $\overline{\lambda}_{trans}$ can be understood as due the absorption and scattering due to λ_i, an effect that is symmetric over the sign of the chirp. The simplifications inherent in the simulation model preclude at this point a definitive assignment of cluster fraction. However, with reasonable confidence we can identify the appearance of the asymmetric blue shift in the chirped incident pulses with optical field ionization of monomers in the cluster jet.

4.3 Effect of Energetic Electrons on the propagation of laser pulses through clustered gas

In this section, we study the kinetic effects of cluster heating and expansion on the propagation of an intense laser pulse through a clustered gas having an effective

dielectric constant determined by the single cluster polarizability. Previously, we had modeled the cluster as a sphere of uniform density modified to match the cluster polarizability from experimentally consistent hydro-code runs and coupled it to a Gaussian description of the laser pulse [72]. This model provided the advantage of computational simplicity over other more complex cluster models [52] [53] and thus was more suited for studying laser propagation through clustered gases where we have to evolve the cluster at many distances and radial zones over the course of the propagation. One of the limitations of the model is that the optical properties of the cluster were entirely determined by the hydrodynamic expansion of the cluster and kinetic effects were entirely absent from the description.

2D and 3D electrostatic Particle-in-Cell (PIC) simulations of argon clusters, of diameter D_0 in the range 20 nm - 53 nm have been done and provide a more sophisticated picture of cluster heating and expansion [53]. These show that at intensity of the order of 5×10^{15} W/cm^2 heating is dominated by a non-linear resonant absorption process. This gives rise to a size dependent intensity threshold beyond which, there is a dramatic increase in the absorption of energy by a small fraction of electrons, creating electrons no longer bound by the cluster potential. These unbound electrons can be expected to contribute to the background electron density forming a tenuous plasma which would effect the laser pulse propagation through the medium.

We modify the description of cluster heating and expansion to include the effect of the unbound electrons based on the predictions of the PIC model [53]. The rate of generation of free electrons is determined by the scaling law of intensity threshold for strong absorption given in reference [53]. Fig 4.4 shows the plot of the

density of free electrons as a function of time within the pulse with peak intensity of 6 $\times 10^{15}$ W/cm^2. Also plotted are the energy absorbed per electron (solid) and the laser pulse intensity profile (arb. units). The density of unbound electrons rises as the electrons are heated by the laser pulse and finally becomes steady towards the end of the pulse.

The polarizability of the cluster is then given by

$$\gamma = \frac{\varepsilon_{\text{cluster}} - 1}{\varepsilon_{\text{cluster}} + 2} \frac{D_0^3}{8} - \frac{n_{unbound}}{4\pi n_{crit}} \tag{4.3}$$

where $\varepsilon_{cluster}$ is the dielectric constant of the cluster, $n_{unbound}$ is the density of electrons escaped from the cluster potential and $n_{crit} = m\omega^2/4\pi e^2$ is the critical density and ω is the laser frequency. The first term on the right hand side of Equation (4.3) is due to the electrons in the cluster core and the second term is due to the unbound electrons.

Fig 4.5 shows the comparison of polarizability results from the 2D PIC code and the modified uniform density code with the inclusion of unbound electrons. The simulations were done for a cluster of initial diameter D_0 = 38 nm. Fig 4.5(a, b) plot the real part of polarizability as a function of time within the pulse for peak intensities ranging from 5×10^{14} W/cm^2 to 1×10^{16} W/cm^2. Fig 4.5(c, d) plot the imaginary part for the same set of peak intensities. For ease of comparison the polarizabilities have been normalized. The polarizability for the PIC case has been normalized to $D_0^2/8$ that is the polarizability per unit length of a metal cylinder of infinite length. For the uniform density case the polarizability is normalized to $D_0^3/8$ that is the polarizability of a uniform dielectric sphere with the dielectric constant tending to infinity. For low

intensities (~1×10^{15} W/cm^2) the cluster polarizability (uniform density case) is determined primarily by the first term in Equation (4.3). The initial positive rise in the polarizability at around 50fs is due to the ionization of the cluster. The polarizability rises as the cluster gets heated and expands. However, as the cluster expands, the density of the cluster electrons falls leading finally to a decreasing polarizability curve. For higher intensities, the free electrons are produced at a higher rate and thus the second term increasingly becomes more important. Thus the positive excursion of polarizability due to cluster expansion is countered by the generation of unbound electrons. This is apparent in the polarizability curve for 4×10^{15} W/cm^2. For even higher intensities, the density of free electrons overwhelms the effect of the expanding cluster and the polarizability drops to negative values very early in the pulse. There is general agreement in the basic time evolution of polarizability from the uniform density model to that computed from the PIC model. The polarizability from PIC code also shows very strong positive excursions at latter times in the pulse. This is due to the oscillation of a halo of bound energetic electrons in the anharmonic potential of cluster ions. The modified uniform density model does not capture this effect. However, we should also note that this occurs at later times in the pulse when there is less power in the pulse.

In order to numerically simulate laser pulse propagation through the clustered gas medium with the inclusion of hot electrons we follow the process outlined in Section3.5, except that we now use the modified cluster polarizability specified by Equation(4.3). The initial parameter values for the cluster and laser field are given in Table 4.1.

Fig 4.6 shows the effect of hot electrons on the evolution of the laser RMS spot size with distance of propagation. Plotted are the RMS spot size of a laser pulse propagating without (filled circles) and with (circles) hot electrons at a peak initial intensity of 1×10^{16} W/cm^2. The evolution of the RMS spot size of an identical pulse propagating in vacuum is provided for comparison. We note that the RMS spot size for the case when cluster expansion is entirely hydrodynamic follows the trend for the spot size evolution at specific ξ positions shown in Fig 3.11(a) and has been discussed in Section 3.5. We note that the inclusion of hot electrons (circles) leads to an increase in the RMS spot size. This is due to the additional defocusing effect of the unbound electrons that act as a low-density background plasma. Since the intensity is peaked on axis, the density of free electrons generated is maximum on-axis and falls off with increasing radial distance. This contributes a positive value to the radial gradient of the effective refractive index leading to a defocusing effect. With propagation, the laser pulse intensity decreases due to absorption leading to a decrease in the free electron density and the pulse starts to self-focus due to the focusing effect of the positive real part of the cluster polarizability and finally at z = 1.2 the RMS spot size is almost equal for either case.

Fig 4.7 plots the evolution of the RMS spot size for peak laser intensity ranging from 1×10^{15} W/cm^2 to 1×10^{17} W/cm^2. Here, the RMS spot size is calculated for that portion of the pulse that contains 90% of the pulse power starting from the front end of the pulse. The evolution of the spot size in vacuum and that in unclustered argon gas (only monomers) for a peak laser intensity of 1×10^{17} W/cm^2 are provided for comparison. We note that the RMS spot size is higher for a higher

peak laser intensity. In other words, there is less focusing. At the intensity of 1×10^{15} W/cm^2 which is below the threshold for strong heating very few unbound electrons are generated and the pulse experiences focusing due to the positive real part of cluster polarizability. As higher intensities there is increased production of unbound electrons that add to the defocusing effect. Thus we see the RMS spot size increase with intensity at any given propagation distance. At the peak intensities of 5×10^{16} W/cm^2 and 1×10^{17} W/cm^2 the pulse RMS spot size is much greater than that in vacuum. However, we note that the RMS spot size for the case of propagation through only monomers is still higher for in that case the focusing effect of the expanding clusters is entirely absent.

4.4 Conclusion

In conclusion, we have presented spectral evidence of the evolution of the laser-heated cluster polarizability during intense pulse propagation in cluster jets. The results confirm our model of cluster evolution, in which the onset of increasing polarizability is accompanied by red shifts, and these red shifts are intimately related to our previous observations of self-focusing. Comparison of the scattered and transmitted spectra of chirped pump pulses also leads to the conclusion that the cluster jet has a non-negligible concentration of monomers, which contribute to a blue shift. Both effects are supported by idealized simulations of pulse propagation in cluster jets.

We also numerically simulate the propagation of laser pulses through clustered gases allowing for the generation of unbound electrons via cluster heating. Our results indicate that unbound electrons lead to defocusing of the laser pulse

especially for intensities above the threshold for strong heating. However, the pulse is still more focused than a similar pulse propagating in unclustered gas.

Table 4.1 Initial conditions for simulation of laser pulse propagation through clustered gas allowing for generation of hot electrons

Pulse	Cluster
Wavelength = 800nm	Initial radius = 38nm
Pulse width = 100fs FWHM	Mass of ions = 10 amu
Peak Intensity at vacuum focus = 1×10^{15} - 1×10^{17} W/cm^2	Threshold intensity for ionization = 1×10^{14} W/cm^2
Vacuum Focus at 0.15 cm from z = 0	Degree of ionization = 8
Spot size = 40μm FWHM	Ion density = 1.75×10^{22} cm^{-3} = $10n_{critical}$
Phase(θ) = 0	Cluster density = 8.39×10^{11} cm^{-2}
Curvature(α) = 0	
Energy = 1.93 mJ – 193 mJ	

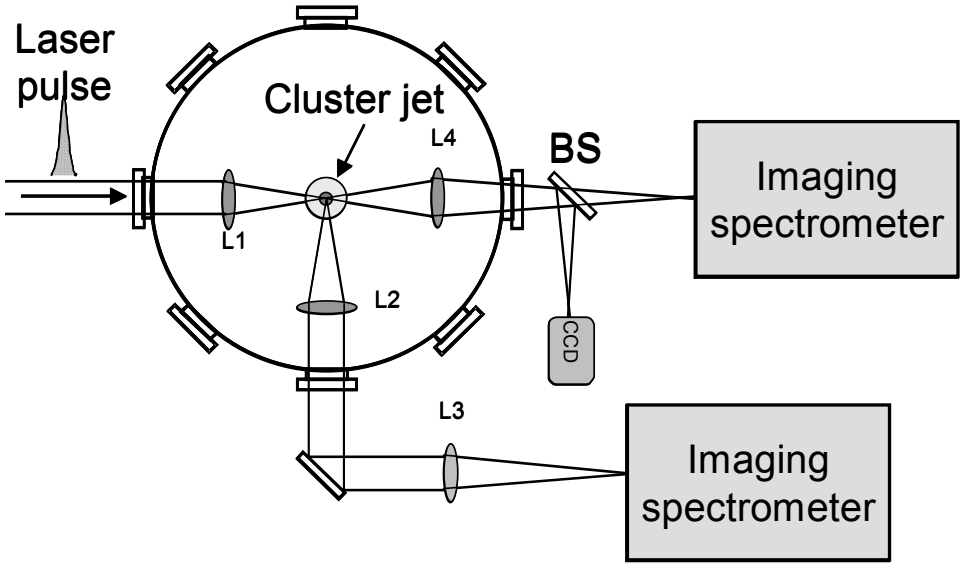

Fig 4.1 Experimental layout for the measurement of forward and side scattered spectra of intense laser pulses interacting with a gas of clusters.

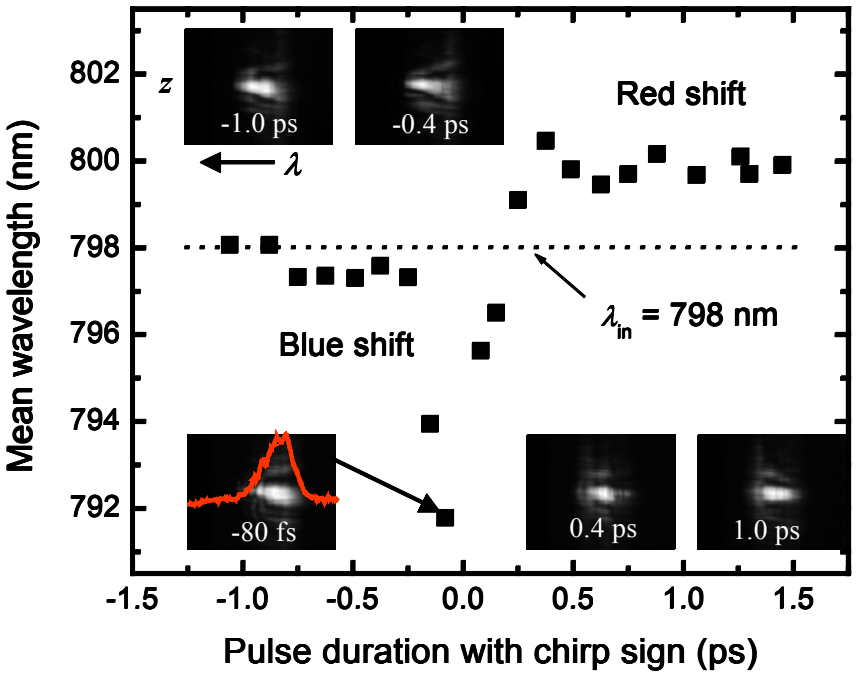

Fig 4.2 Mean wavelength of (a) scattered and (b) transmitted laser pulses as a function of chirped laser pulse durations. The mean wavelength of incident lasers is 798 nm. The insets show sample 1D space-resolved (a) scattering and (b) transmission spectra, respectively.

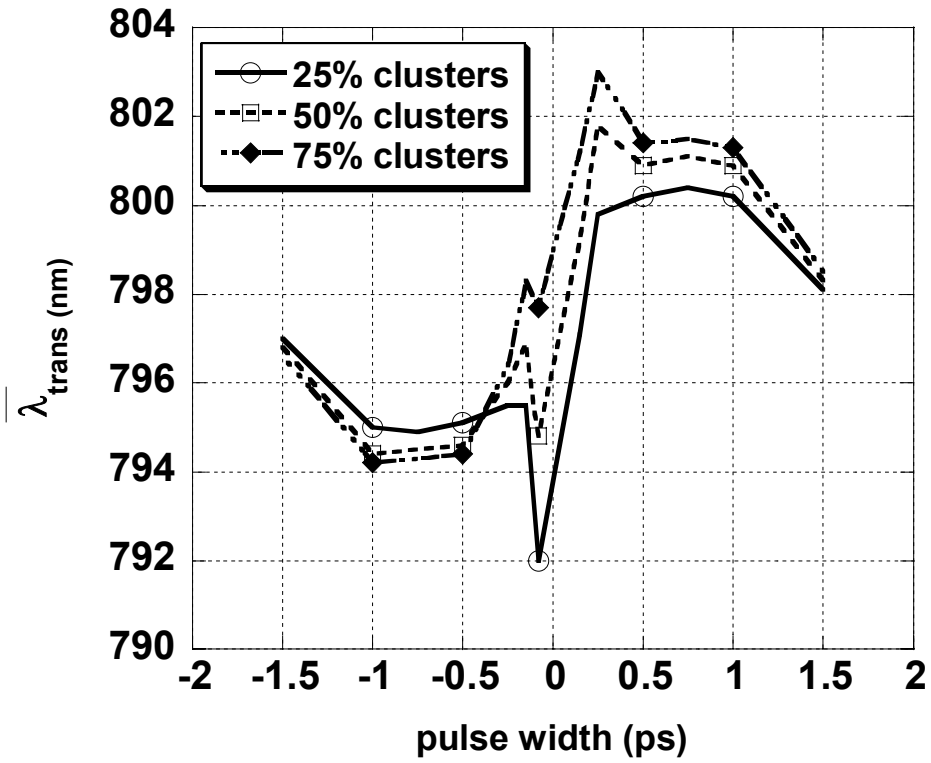

Fig 4.3 Simulated mean wavelength of transmitted laser pulses as a function of chirped laser pulse durations for different assumed fraction of gas atoms present as clusters.

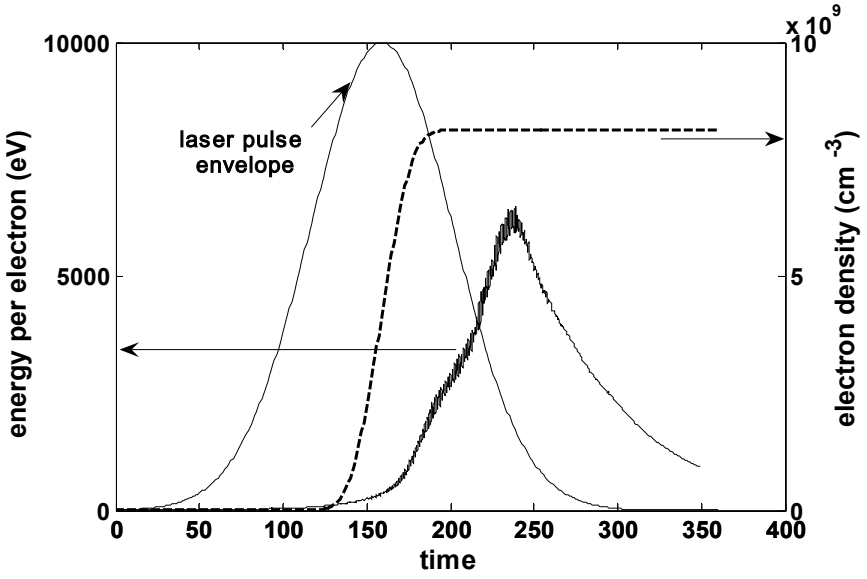

Fig 4.4 The dotted line shows the evolution of free electron density with time within the pulse for peak laser intensity of 6×10^{15} W/cm^2 (the laser pulse envelope is shown in thin solid line). The energy absorbed per electron based on the PIC calculations for the same laser peak intensity is also shown (solid line).

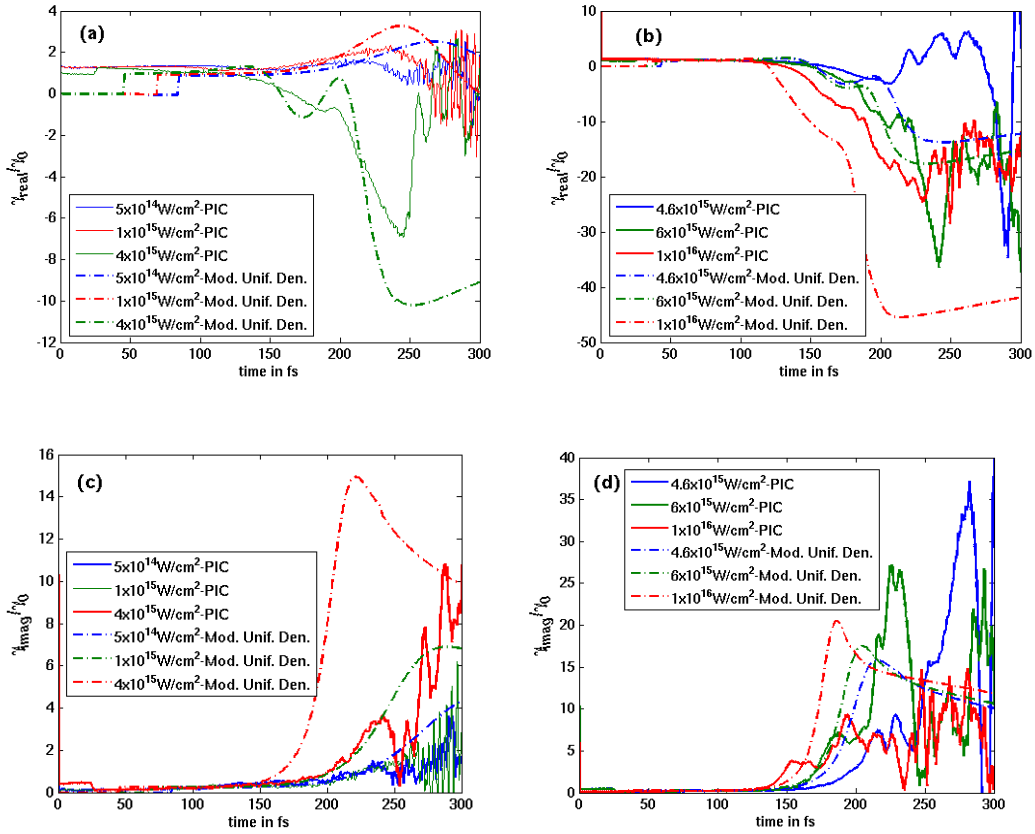

Fig 4.5 Comparison of real (a,b) and imaginary (c,d) parts of cluster polarizability from the PIC code (solid lines) and modified uniform density model of cluster expansion with inclusion of hot electrons (dotted lines) for a range of intensities. For the PIC code the polarizability is normalized to $\gamma_0 = D_0^2/8$, where D_0 is the diameter of the cluster while for the uniform density model it is normalized to $\gamma_0 = D_0^3/8$.

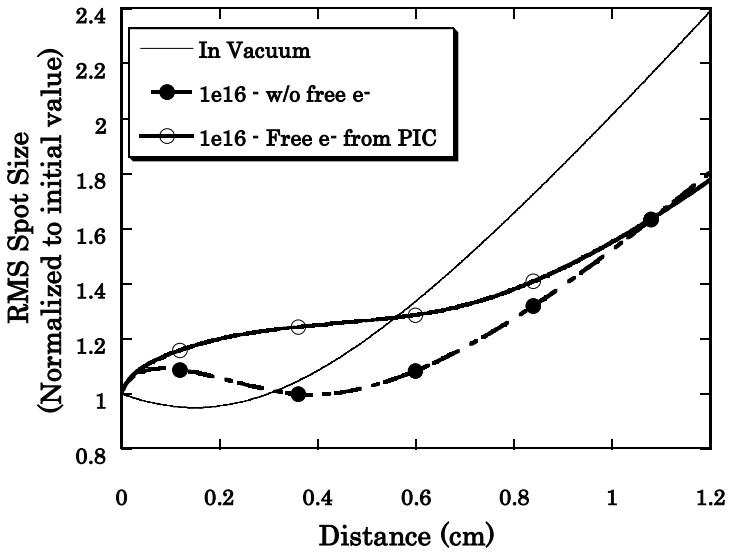

Fig 4.6 RMS spot size of pulse for case when free electrons are included (circles) and when free electrons are not considered (filled circles). The evolution of the RMS spot size for propagation in vacuum is plotted (solid-no marker) for comparison. The free electrons contribute additional defocusing effect.

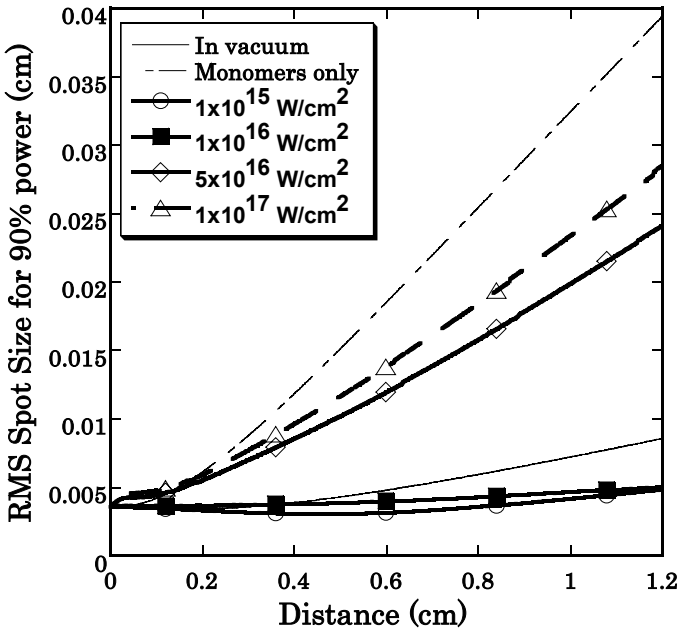

Fig 4.7 RMS spot size of the pulse versus distance of propagation for a range of peak laser intensities. The RMS spot size for propagation in vacuum and through unclustered gas at a peak intensity of 1×10^{17} W/cm^2 is also plotted for comparison. We note that the RMS spot size is higher for higher intensity at any given distance. This is due the generation of more free electrons at higher intensities. However, even for the peak intensity of 1×10^{17} W/cm^2 the RMS spot size is less than that for propagation in vacuum.

5 Summary and Conclusions

In this dissertation, we have studied the interaction of intense laser pulses with gases of nanoscale atomic clusters. Clustered gases act as a unique optical medium intermediate between solids and gases. When irradiated with a laser pulse they absorb the pulse energy very efficiently. The highly efficient coupling of laser energy to clusters leads to many potential applications that have been outlined in Chapter 1. In the first part of the dissertation we investigated the effect of laser pulse duration on cluster heating. We used the 2D electrostatic PIC model of Taguchi and Antonsen [53] that operates in the regime where both kinetic and hydrodynamic effects can contribute to cluster heating and expansion. Our simulations show that the basic heating mechanism is the same as in reference [53] and is dependent on a non-linear 'transit time' resonance of electrons. Electrons are pulled out of the cluster by the laser field and accelerated. The number of laser periods these energetic electrons take to transit once through the cluster defines the order of resonance. For the pulse duration of 100 fs absorption takes place at the lowest order resonance. The onset of this resonance sets up a size-dependent intensity threshold for strong heating (5×10^{15} W/cm^2 for a 38 nm cluster). As we increase the pulse duration, electron phase space plots show that the cluster absorbs energy at higher orders of resonance. We have generalized the formula for predicting the intensity threshold derived by Taguchi [53] to higher order resonances and shown that the threshold intensity for strong heating is inversely proportional to the square of the order of resonance. This explains the lowering of the intensity threshold to 3×10^{15} W/cm^2 as pulse duration is increased

from 100 fs to 250fs. For even higher pulse durations we note that the intensity threshold becomes less dramatic. This is because at pulse lengths of the order of 1 ps, the cluster can spend very long times at high order resonances leading to significant absorption when the intensity is low. Cluster heating at low intensities also leads to cluster expansion earlier in the pulse leading to deviations from the threshold predicted by our generalized formula. One of the limitations of our generalized formula is that it assumes that the cluster does not significantly expand before the peak of the pulse, which does not hold for very long pulse lengths. We study the electron and ion kinetic energy distribution for different pulse duration and peak laser intensities. The ion energy distribution is beamlike and is dominated by a quasi-mono-energetic peak. For both ions and electrons the maximum energy peaks for the 250 fs pulse duration and is lower for both larger and smaller pulse lengths. We also compute the neutron yield from collisions of high-energy ions produced from intense field exploded deuterium clusters.

In the next section of the dissertation, we have developed a self-consistent model for laser pulse propagation through a gas of atomic clusters. For computational simplicity we modeled each cluster as an evolving spherical ball of nanoplasma with uniform density and temperature. This was then coupled to a Gaussian description of the laser pulse. We have also studied stability and equilibrium of the system. Our analysis shows that there are multiple stable and unstable equilibriums. In addition, for a pulse of given energy, a minimum density of clusters is required to maintain equilibrium. Our simulation results indicate that the transient evolution of complex cluster polarizability leads to the self-focusing of the pulse for distances of the order

of 1.5 cm. Such self-guiding of the pulse in clustered gases has been experimentally observed for the parameter range that we considered. Also, our results show almost 80% absorption of the pulse energy by the time the pulse propagates through 1.5 cm. This is also in agreement with experimental measurements of energy absorption by clusters. The temporal variation of the complex cluster polarizability leads to frequency shifts in the transmitted spectrum of the pulse. We have done simulations to mimic the experimental conditions of reference [37]. For this, we allowed for a fraction of the gas to remain unclustered. We incorporated the effect of background plasma formed by the ionization of these monomers on laser pulse propagation. Our simulations explained the observed red shifts for positively chirped laser pulses with long pulse durations and the blue shift observed for short positively chirped pulses. Our results indicate that there is a high percentage of monomers in the cluster jet. Direct experimental measurement of what fraction of the gas is unclustered has not been done yet and would be welcome.

Finally, we extend our fluid description of the cluster heating to include the effect of hot electrons predicted by the PIC model. We have used this modified cluster description to study the effect of hot electrons on laser pulse propagation. Our results show that the escalated production of free electrons for intensities beyond the threshold leads to defocusing of the pulse. However, even for intensities as high as 1×10^{17} W/cm^2 the pulse is more focused than a similar pulse propagating through unclustered gas.

6 Bibliography

1. Hagena, O.F. and W. Obert, *Cluster Formation in Expanding Supersonic Jets - Effect of Pressure, Temperature, Nozzle Size, and Test Gas.* Journal of Chemical Physics, 1972. **56**(5): p. 1793.
2. Ditmire, T., et al., *High intensity laser absorption by gases of atomic clusters.* Physical Review Letters, 1997. **78**(16): p. 3121-3124.
3. Kim, K.Y., et al., *Gases of exploding laser-heated cluster nanoplasmas as a nonlinear optical medium.* Physics of Plasmas, 2004. **11**(5): p. 2882-2889.
4. Ditmire, T., et al., *Strong X-Ray-Emission from High-Temperature Plasmas Produced by Intense Irradiation of Clusters.* Physical Review Letters, 1995. **75**(17): p. 3122-3125.
5. Glenn, D.K., et al. *Scale-up of a cluster jet laser plasma source for extreme ultraviolet lithography*. 1999: SPIE.
6. Feng, J., et al. *Characterization of a laser plasma water droplet EUV source*. 1995: SPIE.
7. Parra, E., et al., *X-ray and extreme ultraviolet emission induced by variable pulse-width irradiation of Ar and Kr clusters and droplets.* Physical Review E (Statistical Physics, Plasmas, Fluids, and Related Interdisciplinary Topics), 2000. **62**(5): p. R5931-R5934.
8. Mori, M., et al., *Extreme ultraviolet emission from Xe clusters excited by high-intensity lasers.* Journal of Applied Physics, 2001. **90**(7): p. 3595-3601.
9. Ter-Avetisyan, S., et al., *Absolute extreme ultraviolet yield from femtosecond-laser-excited Xe clusters.* Physical Review E (Statistical, Nonlinear, and Soft Matter Physics), 2001. **64**(3): p. 036404.
10. Zachary, H.L., et al., *Tomographic reconstruction of an integrated circuit interconnect.* Applied Physics Letters, 1999. **74**(1): p. 150-152.
11. Shao, Y.L., et al., *Multi-keV electron generation in the interaction of intense laser pulses with xe clusters.* Physical Review Letters, 1996. **77**(16): p. 3343-3346.
12. Ditmire, T., et al., *Nuclear fusion from explosions of femtosecond laser-heated deuterium clusters.* Nature, 1999. **398**(6727): p. 489-492.
13. Kumarappan, V., M. Krishnamurthy, and D. Mathur, *Asymmetric high-energy ion emission from argon clusters in intense laser fields.* Physical Review Letters, 2001. **87**(8): p. 085005.
14. Fourkal, E., et al., *Intensity modulated radiation therapy using laser-accelerated protons: a Monte Carlo dosimetric study.* Physics in Medicine and Biology, 2003. **48**(24): p. 3977-4000.
15. Madison, K.W., et al., *Investigation of fusion yield from exploding deuterium-cluster plasmas produced by 100-TW laser pulses.* Journal of the Optical Society of America B-Optical Physics, 2003. **20**(1): p. 113-117.
16. Donnelly, T.D., et al., *High-order harmonic generation in atom clusters.* Physical Review Letters, 1996. **76**(14): p. 2472-2475.

17. Alexeev, I., et al., *Self-focusing of intense laser pulses in a clustered gas.* Physical Review Letters, 2003. **90**: p. 103402.
18. Ditmire, T., R.A. Smith, and M.H.R. Hutchinson, *Plasma waveguide formation in predissociated clustering gases.* Optics Letters, 1998. **23**(5): p. 322-324.
19. Kumarappan, V., K.Y. Kim, and H.M. Milchberg, *Guiding of intense laser pulses in plasma waveguides produced from efficient, femtosecond end-pumped heating of clustered gases.* Physical Review Letters, 2005. **94**: p. 205004.
20. Borisov, A.B., et al., *Multielectron motions induced in clusters and molecules in self-trapped channels.* Multiphoton Processes 1996, 1997(154): p. 1-9.
21. Mcpherson, A., et al., *Multiphoton Induced X-Ray-Emission from Kr Clusters on M-Shell (Similar-to-100-Angstrom) and L-Shell (Similar-to-6-Angstrom) Transitions.* Physical Review Letters, 1994. **72**(12): p. 1810-1813.
22. Mcpherson, A., et al., *Multiphoton-Induced X-Ray-Emission and Amplification from Clusters.* Applied Physics B-Photophysics and Laser Chemistry, 1993. **57**(5): p. 337-347.
23. Mcpherson, A., et al., *Multiphoton-Induced X-Ray-Emission and Amplification from Clusters (Vol 57, Pg 337, 1993).* Applied Physics B-Lasers and Optics, 1994. **58**(4): p. 343-343.
24. Mcpherson, A., et al., *Multiphoton-Induced X-Ray-Emission at 4-5 Kev from Xe Atoms with Multiple Core Vacancies.* Nature, 1994. **370**(6491): p. 631-634.
25. Ditmire, T., et al., *X-ray yields from Xe clusters heated by short pulse high intensity lasers.* Applied Physics Letters, 1997. **71**(2): p. 166-168.
26. Eisuke, M., et al. *X-ray emissions from clusters excited by ultrashort laser pulses*. 2000: SPIE.
27. Parra, E., et al., *X-ray and extreme ultraviolet emission induced by variable pulse-width irradiation of Ar and Kr clusters and droplets.* Physical Review E, 2000. **62**(5): p. R5931-R5934.
28. Anatoly, Y.F., et al. *X-ray radiation properties of clusters heated by fs laser pulses*. 2001: SPIE.
29. J. Abdallah, Jr., et al., *Hot-electron influence on the x-ray emission spectra of Ar clusters heated by a high-intensity 60-fs laser pulse.* Physical Review A (Atomic, Molecular, and Optical Physics), 2001. **63**(3): p. 032706.
30. Kumarappan, V., et al., *Effect of laser polarization on x-ray emission from Ar-n (n=200-10(4)) clusters in intense laser fields.* Physical Review A, 2001. **6302**: p. 023203.
31. Tomas, M., et al. *Soft x-ray emission from Ar clusters heated by ultrashort laser pulse*. 2001: SPIE.
32. Junkel-Vives, G.C., et al., *Spatially resolved x-ray spectroscopy investigation of femtosecond laser irradiated Ar clusters.* Physical Review E (Statistical, Nonlinear, and Soft Matter Physics), 2002. **65**(3): p. 036410.
33. Mocek, T., et al. *Enhanced X-ray Emission from Nitrogen Clusters Ionized by Intense, Ultrashort Laser Pulses*. 2002: AIP.

34. Shiraishi, T., M. Mori, and K. Kondo, *Estimation of the pulse width of x-ray emission from Xe clusters excited by a subpicosecond intense Ti:sapphire laser pulse.* Physical Review A (Atomic, Molecular, and Optical Physics), 2002. **65**(4): p. 045201.
35. Toma, E.S. and H.G. Muller, *X-ray emission after laser disintegration of clusters of carbon-containing molecules.* Physical Review A (Atomic, Molecular, and Optical Physics), 2002. **66**(1): p. 013205.
36. Yuji, F., et al. *X-ray radiation of clusters irradiated by ultrafast high-intensity laser pulses*. 2004: SPIE.
37. Kim, K.Y., et al., *Spectral redshifts in the intense laser-cluster interaction.* Physical Review A, 2005. **71**: p. 011201.
38. Tisch, J.W.G., et al., *Investigation of high-harmonic generation from xenon atom clusters.* Journal of Physics B-Atomic Molecular and Optical Physics, 1997. **30**(20): p. L709-L714.
39. Tisch, J.W.G., et al., *High-harmonic generation from xenon atom clusters.* Multiphoton Processes 1996, 1997(154): p. 177-185.
40. Ditmire, T., et al., *High-energy ions produced in explosions of superheated atomic clusters.* Nature, 1997. **386**(6620): p. 54-56.
41. Zweiback, J., et al., *Nuclear fusion driven by Coulomb explosions of large deuterium clusters.* Physical Review Letters, 2000. **84**(12): p. 2634-2637.
42. Kim, K.Y., V. Kumarappan, and H.M. Milchberg, *Measurement of the average size and density of clusters in a gas jet.* Applied Physics Letters, 2003. **83**(15): p. 3210-3212.
43. Springate, E., et al., *Explosion of atomic clusters irradiated by high-intensity laser pulses: Scaling of ion energies with cluster and laser parameters.* Physical Review A, 2000. **61**: p. 063201.
44. Madison, K.W., et al., *Fusion neutron and ion emission from deuterium and deuterated methane cluster plasmas.* Physics of Plasmas, 2004. **11**(1): p. 270-277.
45. Rose-Petruck, C., et al., *Ultrafast electron dynamics and inner-shell ionization in laser driven clusters.* Physical Review A, 1997. **55**(2): p. 1182.
46. Ishikawa, K. and T. Blenski, *Explosion dynamics of rare-gas clusters in an intense laser field.* Physical Review A, 2000. **62**: p. 063204.
47. Petrov, G.M., et al., *Modeling of clusters in a strong 248-nm laser field by a three-dimensional relativistic molecular dynamic model.* Physical Review E, 2005. **71**: p. 036411.
48. Petrov, G.M., et al., *Dynamics of a Xe cluster plasma produced by an intense ultrashort pulse KrF laser.* Physics of Plasmas, 2005. **12**: p. 063103.
49. Eloy, M., et al., *MeV ions generated via coulombic explosions of atomic clusters.* Physica Scripta, 2001. **T89**: p. 60-62.
50. C. K. Birdsall, A.B.L., *Plasma Physics via Computer Simulation*. 1985 ed. 1985: McGraw-Hill, New York.
51. Ditmire, T., et al., *Interaction of intense laser pulses with atomic clusters.* Physical Review A, 1996. **53**(5): p. 3379-3402.
52. Milchberg, H.M., S.J. McNaught, and E. Parra, *Plasma hydrodynamics of the intense laser-cluster interaction.* Physical Review E, 2001. **64**: p. 056402.

53. Taguchi, T., T.M. Antonsen, and H.M. Milchberg, *Resonant heating of a cluster plasma by intense laser light.* Physical Review Letters, 2004. **92**: p. 205003.
54. Antonsen, T.M., et al., *Resonant heating of a cluster plasma by intense laser light.* Physics of Plasmas, 2005. **12**(5): p. -.
55. Greschik, F. and H. Kull, *Two-dimensional PIC simulation of atomic clusters in intense laser fields.* Laser and Particle Beams, 2004. **22**(2): p. 137-145.
56. Breizman, B.N., A.V. Arefiev, and M.V. Fomyts'kyi, *Nonlinear physics of laser-irradiated microclusters.* Physics of Plasmas, 2005. **12**: p. 056706.
57. Brunel, F., *Not-So-Resonant, Resonant Absorption.* Physical Review Letters, 1987. **59**(1): p. 52-55.
58. Fomyts'kyi, M.V., et al., *Harmonic generation in clusters.* Physics of Plasmas, 2004. **11**(7): p. 3349-3359.
59. Liu, J.S., et al., *Modified hydrodynamic model and its application in the investigation of laser-cluster interactions.* Physical Review A, 2001. **64**: p. 033426.
60. Zharova, N.A., A.G. Litvak, and V.A. Mironov, *Self-focusing of laser radiation in cluster plasma.* Jetp Letters, 2003. **78**(10): p. 619-623.
61. Madison, K.W., et al., *Role of laser-pulse duration in the neutron yield of deuterium cluster targets.* Physical Review A, 2004. **70**: p. 053201.
62. Zweiback, J., et al., *Detailed study of nuclear fusion from femtosecond laser-driven explosions of deuterium clusters.* Physics of Plasmas, 2002. **9**(7): p. 3108-3120.
63. Kishimoto, Y., T. Masaki, and T. Tajima, *High energy ions and nuclear fusion in laser-cluster interaction.* Physics of Plasmas, 2002. **9**(2): p. 589-601.
64. Singhal, H., et al., *Spectral blueshifts in laser light scattered from argon-gas-cluster plasmas.* Physical Review A, 2005. **72**: p. 043201.
65. Greschik, F., L. Arndt, and H.J. Kull, *Absorption of few-cycle laser pulses by outer ionization of atomic clusters.* Europhysics Letters, 2005. **72**(3): p. 376-382.
66. Zweiback, J., T. Ditmire, and M.D. Perry, *Resonance in scattering and absorption from large noble gas clusters.* Optics Express, 2000. **6**(12): p. 236-242.
67. Schnurer, M., et al., *Influence of laser pulse width on absolute EUV-yield from Xe-clusters.* European Physical Journal D, 2001. **14**(3): p. 331-335.
68. Gupta, A., et al., *Effect of Pulse Duration on Resonant Heating of Argon and Deuterium Clusters.* Physical Review E, (Submitted for Review, July 2006).
69. Miley, G.H., H. Towner, and N. Ivich, *Fusion Cross Section and Reactivities*, in *Rept. COO-2218-17*. 1974, University of Illinois, Urbana, IL.
70. Duane, B.H., *Fusion Cross Section Theory*, in *Rept. BNWL-1685*. 1972, Brokhaven National Laboratory.
71. Caillaud, T., et al., *Study of intense femtosecond laser propagation into a dense Ar gas and cluster jet.* Physics of Plasmas, 2006. **13**: p. 033105.
72. Gupta, A., T.M. Antonsen, and H.M. Milchberg, *Propagation of intense short laser pulses in a gas of atomic clusters.* Physical Review E, 2004. **70**: p. 046410.

73. Kim, K.Y., et al., *Time-resolved explosion of intense-laser-heated clusters.* Physical Review Letters, 2003. **90**: p. 023401.
74. Zweiback, J., T. Ditmire, and M.D. Perry, *Femtosecond time-resolved studies of the dynamics of noble-gas cluster explosions.* Physical Review A, 1999. **59**(5): p. R3166-R3169.
75. Eloy, M., et al., *Interaction of ultrashort high-intensity laser pulses with atomic clusters.* Physics of Plasmas, 2001. **8**(3): p. 1084-1086.
76. Gupta, A. *Self Focusing in Cluster Plasma*. in *43rd Annual Meeting of the Division of Plasma Physics*. 2001. Long Beach, California: American Physical Society.
77. Fomichev, S.V., et al., *Laser-induced nonlinear excitation of collective electron motion in a cluster.* Journal of Physics B-Atomic Molecular and Optical Physics, 2003. **36**(18): p. 3817-3834.
78. Jackson, J.D., *Classical Electrodynamics*. Third Edition ed. 1999: John Wiley & Sons, Inc.
79. Lyman Spitzer, J., *Physics of Fully Ionized Gases*. Second Revised Edition ed. 1962: Interscience Publishers.
80. Esarey, E., et al., *Self-focusing and guiding of short laser pulses in ionizing gases and plasmas.* Ieee Journal of Quantum Electronics, 1997. **33**(11): p. 1879-1914.
81. Watts, I., et al., *Measurements of relativistic self-phase-modulation in plasma.* Physical Review E, 2002. **66**: p. 036409.
82. Max, C.E., J. Arons, and A.B. Langdon, *Self-Modulation and Self-Focusing of Electromagnetic-Waves in Plasmas.* Physical Review Letters, 1974. **33**(4): p. 209-212.
83. Wood, W.M., C.W. Siders, and M.C. Downer, *Measurement of Femtosecond Ionization Dynamics of Atmospheric Density Gases by Spectral Blueshifting.* Physical Review Letters, 1991. **67**(25): p. 3523-3526.
84. Kim, K.Y., I. Alexeev, and H.M. Milchberg, *Single-shot measurement of laser-induced double step ionization of helium.* Optics Express, 2002. **10**(26): p. 1563-1572.
85. Liu, J.S., et al., *Cluster explosion investigated by linearly chirped spectral scattering of an expanding plasma sphere.* Physical Review A, 2006. **73**: p. 033201.
86. Gupta, A. *Intense Laser Cluster Interaction: Effect of Hot Electrons on Propagation and Studies with Longer Pulse Widths*. in *47th Annual Meeting of the Division of Plasma Physics, American Physical Society*. 2005. Denver, Colorado: American Physical Society.
87. Ammosov, M.V., N.B. Delone, and V.P. Krainov, *Tunnel Ionization of Complex Atoms and Atomic Ions in a Varying Electromagnetic-Field.* Zhurnal Eksperimentalnoi I Teoreticheskoi Fiziki, 1986. **91**(6): p. 2008-2013.